

Review

Research Progress in Metal-Organic Framework Based Nanomaterials Applied in Battery Cathodes

Maria Mechili ¹, Christos Vaitsis ¹, Nikolaos Argirusis ², Pavlos K. Pandis ¹, Georgia Sourkouni ³,
Antonis A. Zorpas ^{4,*} and Christos Argirusis ^{1,3,*}

¹ Laboratory of Inorganic Materials Technology, School of Chemical Engineering, National Technical University of Athens, 9 Heroon Polytechniou Str., Zografou, 15780 Athens, Greece; marymehilli@gmail.com (M.M.); vaitsis@central.ntua.gr (C.V.); ppandis@chemeng.ntua.gr (P.K.P.)

² mat4nrg GmbH, Burgstätter Str. 42, 38678 Clausthal-Zellerfeld, Germany; nikos.argirusis@mat4nrg.de

³ TU Clausthal, Clausthaler Zentrum für Materialtechnologie, Leibnizstr. 9, 38678 Clausthal-Zellerfeld, Germany; cogsa@tu-clausthal.de

⁴ Laboratory of Chemical Engineering and Engineering Sustainability, Faculty of Pure and Applied Sciences, Open University of Cyprus, 33 Giannou Kranidioti Ave., Latsia, Nicosia 2220, Cyprus

* Correspondence: antoniszorpas@yahoo.com (A.A.Z.); amca@chemeng.ntua.gr (C.A.)

Abstract: Metal-Organic Frameworks have attracted profound attention the latest years for use in environmental applications. They can offer a broad variety of functions due to their tunable porosity, high surface area and metal activity centers. Not more than ten years ago, they have been applied experimentally for the first time in energy storage devices, such as batteries. Specifically, MOFs have been investigated thoroughly as potential materials hosting the oxidizing agent in the cathode electrode of several battery systems such as Lithium Batteries, Metal-Ion Batteries and Metal-Air Batteries. The aim of this review is to provide researchers with a summary of the electrochemical properties and performance of MOFs recently implemented in battery cathodes in order to provide fertile ground for further exploration of performance-oriented materials. In the following sections, the basic working principles of each battery system are briefly defined, and special emphasis is dedicated to MOF-based or MOF-derived nanomaterials, especially nanocomposites, which have been tested as potential battery cathodes.

Keywords: metal-organic frameworks; battery; cathodes; electrocatalyst; lithium battery; nanomaterials; nanocomposites



Citation: Mechili, M.; Vaitsis, C.; Argirusis, N.; Pandis, P.K.; Sourkouni, G.; Zorpas, A.A.; Argirusis, C. Research Progress in Metal-Organic Framework Based Nanomaterials Applied in Battery Cathodes. *Energies* **2022**, *15*, 5460. <https://doi.org/10.3390/en15155460>

Academic Editor: Cai Shen

Received: 3 July 2022

Accepted: 23 July 2022

Published: 28 July 2022

Publisher's Note: MDPI stays neutral with regard to jurisdictional claims in published maps and institutional affiliations.



Copyright: © 2022 by the authors. Licensee MDPI, Basel, Switzerland. This article is an open access article distributed under the terms and conditions of the Creative Commons Attribution (CC BY) license (<https://creativecommons.org/licenses/by/4.0/>).

1. Introduction

Continuously expanding energy demands constitute one of the most crucial worldwide concerns. Batteries offer a viable solution to store power deriving from renewable energy sources, however, there are still challenges regarding the environmental footprint and the abundance of resources of batteries when taking into account the production route and their disposal.

Primary and rechargeable batteries' performance is closely related to the efficiency and durability of the oxidizing material, contained in the cathode. In general, cathodes need to present ionic and electronic conductivity, mechanical and chemical endurance, rechargeability and of course nontoxicity and safety, like all battery electrodes. For all those requirements to be met while enhancing the battery's performance, researchers have been developing over the years more and more delicate solutions which offered highly functional materials. However, current worldwide material and energy restrictions demand dramatic reductions of complexity and value of the solutions proposed for future upscale. In other words, synthesis procedures need to be simplified, materials used have to be widely accessible and cost-effective and all the processes of cathode manufacture should meet current requirements of environmental friendliness [1–5].

Metal-Organic Frameworks (MOFs) have attracted much interest in energy applications due to the ample unique geometries and porosity they can acquire which lead to distinct electrochemical properties [1,6]. Their synthesis routes have been identified as scalable, while they have proved to be highly versatile when forming hybrids. MOFs include a considerable variety of different linkers and metals that can be combined, with a significant part of them being receptive to rational modifications in order to bring novel functionalities to the table [7,8]. Nevertheless, one of the main drawbacks of MOFs for electrochemical applications is the low conductivity caused by the organic linkers' inherent insulation and poor overlap between their π orbitals and metal centers d orbital [9,10].

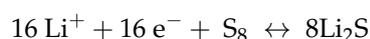
When combined with other nanostructures, MOFs are able to form multifunctional hybrids with abundant active sites exhibiting enhanced electronic and ionic conductivity and electrochemical properties. In such ways, the intrinsic capacity of the electrode can be expanded while the kinetics of redox reactions can be accelerated. MOFs have also been considered as self-sacrifice templates of carbon-based architectures that act as a support for catalytic molecules or even precursors of oxides. Calcination in the air has been very popular for the preparation of metal oxides, whereas pyrolysis in an inert atmosphere can produce hierarchical carbons. The development of methods in order to tailor the morphology and porosity of such materials has been a significant obstacle over the years, thus MOFs can alleviate this with fine-tuning during the initial synthesis. The atomically homogeneous structure ensures a uniform distribution between the carbon and the metal-based part, which can also be removed completely via acid treatments. The generation of such intriguing designs can ameliorate the cycling stability and overall battery performance [11].

This review aims to give an overview of MOF-based nanomaterials and nanocomposites, applied in battery cathodes, giving emphasis to innovative MOF conjunctions. In the first place, an overview of pristine MOFs is provided, while afterward the properties of MOFs derivatives and their nanocomposites are summarized. The materials are organized depending on the battery application as Lithium batteries, Metal-Ion batteries, and Metal-Air batteries (MABs) have diverse operational demands.

2. Lithium Batteries

When referring to Lithium Batteries we describe batteries with Li anodes and porous cathodes accommodating Sulfur (or Selenium) as an active material. Their fundamental operation lies in the transfer of lithium ions towards the confined Sulfur in the cathode, in order to form lithium sulfide via several redox reactions and intermediates [12].

The overall electrochemical reaction can be summarized below:



Their theoretical capacity reaches relatively high numbers (1C = 1672 mAh/g) however they suffer from a destructive phenomenon known as the shuttle effect. Shuttle Effect describes the corrosive mobility of intermediate polysulfides towards the anode and back, leading to self-discharge and early stability fade. These short-chain polysulfides can be mitigated by more efficient encapsulation of sulfur in the cathode pores. MOFs have been thoroughly explored as potential hosts due to their extended surface area and pore structure, including carbon derivatives which possess higher electrical conductivity and mechanical flexibility [13–17].

The first attempt to insert a MOF in a Lithium- Sulfur (Li-S) battery cathode goes back to 2011 and MIL-100 (Cr). MIL-100 (Cr) is based on trimesic acid linker and chromium octahedra, possessing mesoporous cages of 25–29 Å and pore volume of $\sim 1 \text{ cm}^3/\text{g}$. For the preparation of the cathode at least 25 wt% of carbon was needed to increase the conductivity while the integration of Sulfur took place at 155 °C (melting point of 115 °C). The cathode capacity did not exceed 500 mAh/g after 50 cycles probably due to the fragile binding of polysulfide anions to the framework or blockage of sulfur from the carbon matrix [18]. The corresponding vanadium variant was also applied for 200 cycles at 0.1C, delivering a

reversible capacity of ~550 mAh/g, along with a reduced graphene oxide (RGO) composite, which demonstrated a slightly enhanced efficiency with 650 mAh/g at 0.1C after 75 cycles and 450 mAh/g over 300 cycles at 0.5C, albeit not directly comparative results [19].

Particle size proved to acquire a principal role among other parameters concerning the capacity of the cathode. Baumann et al. [20] modified the particle size of HKUST-1 and studied the effect on battery performance. The samples were of particle sizes 0.16, 1.6, and 5.9 μm samples and delivered correspondingly 679, 540 and 480 mAh/g and capacity retentions of 64, 60 and 54% (end of 20 cycles at 0.1C). It is highlighted that an autoclave-free “precooling” procedure was followed in order to synthesize the nanosized MOFs (0.16 nm) which showed the most favorable electrochemical properties. Furthermore, the features of ZIF-8 were extensively investigated when nanosizing [20]. Zhou et al. [21] prepared particles of 2 μm , 800 nm, 200 nm, 70 nm and 15 nm via a facile solution synthesis route and reported their long-term stability for 250 cycles at 0.5 C. The cathode comprised of the MOF NPs of 15 nm delivered the highest maximum capacity 968 mAh/g. One year before, the same team conducted similar research also for HKUST-1, MIL-53 (Al) and NH_2 -MIL-53 (Al). Although the capacities noted for ZIF-8 were significantly lower, the results verified that downsizing particles benefit sulfur utilization due to the larger total external surface area and shorter electron diffusion pathway for sulfur species reduction in the framework. Among the above MOFs, MIL-53 exhibited the best performance, reaching a discharge capacity of 793 mAh/g and maintaining 44% of the capacity over 300 cycles at 0.5C. Geng et al. [22] recently conducted an investigation on which morphological factors have the strongest effect on MIL-96-Al crystals’ performance in a Li-S battery application.

Another strategy reported to enhance sulfur confinement by modifying active surface area is boosting macro and microporosity of ZIF-8 by exploiting PMMA nanospheres as templates and ZnO as a precursor (Figure 1). The 3DOM ZIF-8 presented remarkable stability over 500 galvanostatic cycles at 2C (capacity retention 84%) when applied as a cathode in a Li-S battery. The prohibition of early degradation was attributed to the powerful interaction between 3DOM ZIF and polysulfides, as verified by UV-Vis and XPS analysis [23]. A similar method was followed recently by Wang et al. [24] who utilized a PS template to form a 3DOM ZIF67 matrix to confine Sulfur molecules. The resulted cathode delivered an initial capacity of 1079.8 mAh/g at 0.2C and endured 500 cycles at 1C.

Beyond their role in downsizing, creating heterostructures with carbon conductive substances has been a very popular method to enhance the activity of electrode material. MOFs’ weaknesses can be alleviated by integrating carbon materials, possessing numerous benefits, such as different forms (graphene, nanotubes), high conductivity, mechanical strength and chemical robustness [25]. Regarding GO, it is mainly used in its reduced form. Wang and co-workers studied ZIF-8@rGO as a cathode by firstly preparing the zinc carbonate hydroxide/rGO composite, which was used as a precursor for the final sample [26]. The nanocomposite’s micropores can provide better dispersion of S_8 crowns and the abundant nitrogen sites can immobilize the polysulfides by forming Li-N bonds and enhance cycling stability. At 200 mA/g the cathode supplied a high initial discharge capacity of 1544 mAh/g, retaining at 523 mAh/g at the end of 200 cycles, compared to pure ZIF-8, which delivered 1206 and 346 mAh/g, respectively. On the other hand, setting higher current densities (1 A/g) leads to much lower initial capacities; 678 mAh/g for the composite, and 426 mAh/g for the pristine ZIF-8, after 300 cycles [26].

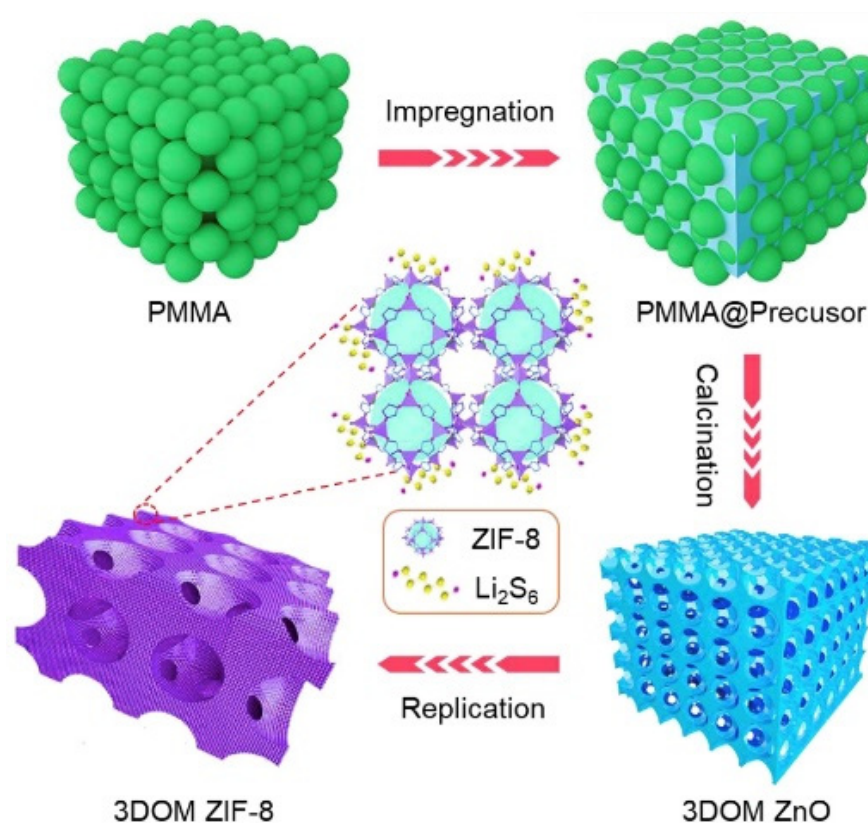


Figure 1. Schematic illustration of 3DOM ZIF-8 synthesis process. Reproduced with permission from [23]. (Copyright Elsevier).

Carbon nanotubes (CNTs) have also been popular due to their high tensile strength, flexibility, conductivity, and aspect ratio. A hollow ZIF-8 (HZIF) with CNTs was reported by Wu et al. by using tannic acid as a modulator [27]. SEM pictures reveal the hollow structure with a shell thickness of 55 nm. Through the electrostatic force, negative charged CNTs are attached to the positive charged HZIF (functionalized with PDDA), to receive the hybrid sulfur host. The polysulfides adsorption was studied with XPS analysis; after the Li_2S_6 adsorption, weaker C-O, C=O and C-N peaks were observed, indicating the strong capture capabilities of O and N functional groups. The cathode (75 wt.% sulfur content) managed to deliver good cycling stability, with a capacity of 625 mAh/g after 500 cycles at 0.5C and promising efficiency at the increased rate of 3C (696 mAh/g) (Figure 2) [27].

Tannic acid was also utilized as a modulator by Ge et al. [28] in an attempt to form a more functional ZIF-67 in order to mitigate the shuttle effect. The idea is that the hydroxyl groups of tannic acid can modify polysulfides into being insoluble. Tannic acid also tends to deform Co-N bonds, promotes the formation of N-H bonds, activates polarity and restricts the dissolution of polysulfide intermediates in the electrolyte [13]. The pristine ZIF-67 delivered a specific capacity of 422 mAh/g for 100 cycles at 100 mA/g, while 5 min of treatment with tannic acid attributed to the battery and raise the capacity to 757 mAh/g.

Turning back to nanocomposites' investigation, Bao et al. prepared mesoporous MIL-101@rGO, which displayed a capacity of 650 mAh/g after 50 cycles at 0.2C with a capacity retention of 66.6% [29]. The mesopores can significantly slow down the shuttle effect, due to the strong adsorption of polysulfides [30]. Additionally, micropores can also prevent the above issue, while promoting the entrapment of elemental sulfur for increased discharge capabilities.

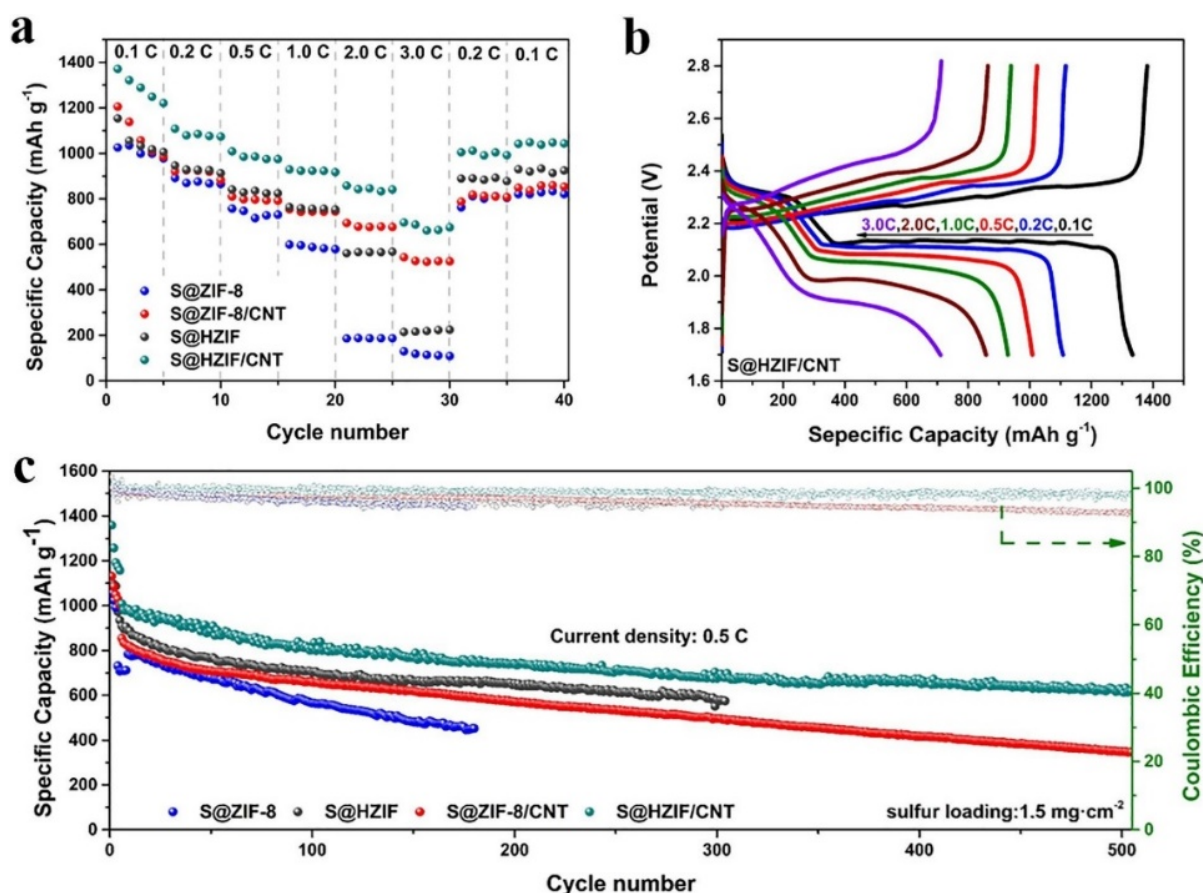


Figure 2. (a) Rate performance at various rates, (b) voltage profiles at various current densities, (c) long-term cycling at 0.5C. Adapted with permission from [27]. (Copyright 2021, Elsevier).

An rGO coating layer can offer a better sulfur utilization rate along with increased conductivity while suppressing the volume expansion throughout the redox reaction. Such an example has been investigated with an iron MOF based on azobenzenetetracarboxylic acid ligand [31]. A faster capacity fade is observed during the first 80 cycles dropping from 1643 to 865 mAh/g and reaching 639 mAh/g after a total of 200 cycles at 0.5C (Figure 3). The high initial capacity of the composite is induced by the layer conductivity and the reduction of the interface contact resistance [32].

Xu et al. synthesized a Ni-MOF-74/CNT composite via a typical solvothermal method [33]. The MOF structure pores could trap the polysulfides, whereas MWCNTs provided the electric path and necessary channels for the electrolyte transfer. The cathode maintained 503 mAh/g after 400 cycles at 2C, with retention of 65.1%. The CNTs concentration is also integral to the final properties and its effect has been tested during the preparation of UiO-66/CNT [34]. Additionally, since an ideal UiO-66 does not have available Lewis acidic sites to bind the polysulfides, benzoic acid was used as a modulator, competing with terephthalic acid and creating linker-missing defects in order to introduce more active sites and receive a more open framework [35–37]. The interaction of coordination defects and polysulfides entrapment was studied with DFT [34]. In short, structures with 1–3 linker defects were simulated, showing not only a stronger affinity to Li_2S_4 than an ideal UiO-66 but an enlargement of inner cavities [36]. However, more defects lead to the opposite effect weakening the binding energy [34]. The composite achieved better cycling stability with 34% CNT content, instead of 23 or 56%, both over 300 cycles at 0.5 A/g (765 mAh/g), and over 800 cycles at 1 A/g (~500 mAh/g).

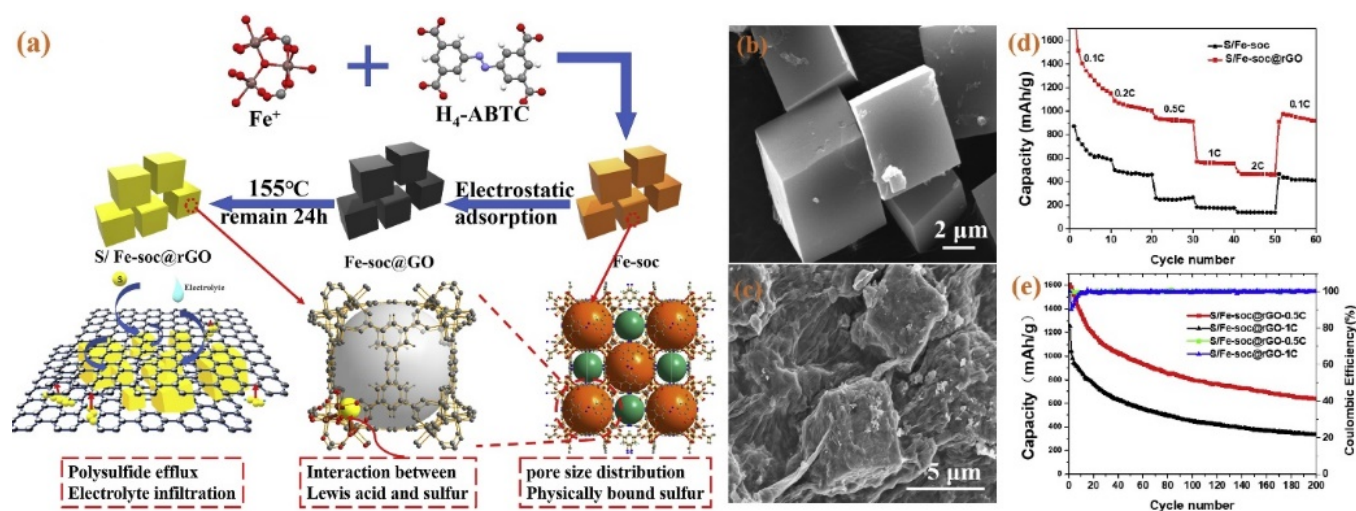


Figure 3. (a) Fe-soc@rGO synthesis scheme, SEM images of (b) Fe-soc (c) Fe-soc@rGO, (d) rate performance, (e) cycle performance. Adapted with permission from [31]. (Copyright 2020, Elsevier).

Further thermal treatment of MOFs can form nanocarbons, which adopt the same morphology as their precursor. This provides researchers with the opportunity to explore a wide variety of unique architectures to confine and stabilize sulfur molecules. These architectures exhibit a conductivity appropriate for utilization in a battery system.

ZIF-8 derived carbons have been an attractive option recently to enclose sulfur, forming morphologies such as typical rhombic dodecahedrons [38–40], spheres [41] and nanosheets [42] or nanocomposites with graphene [43–45] or grown on 1D structures such as CNTs [46] or nanofibers [47] in order to be applied in Li-S cathodes. A successful example has been the production of N-doped hierarchically porous carbon 2D nanosheets by Jiang et al. in order to immobilize sulfur molecules. The fabricated cathode could attain 300 cycles, while in the 100th cycle it delivered capacity retention of 65.2% at 0.2C. The overall battery system supplied an initial capacity of 1226 mAh/g [42].

In the same direction, MOF-5 has been considered an efficient source of Mesoporous carbon for sulfur encapsulation, which has been enriched with metal carbides [48], graphene sheets [49] and MWCNTs [50]. Literature review reveals an extensive exploration of ZIF-67 as a precursor of carbonaceous structures since it can attribute to the material cobalt sites which enhance the sulfur confinement. The corresponding composite architectures can be typical ZIF-67 derived polyhedra [51–54], polyhedra decorated with CNTs [55–58] or combined with graphene structures [32,59,60]. A recent study can be highlighted that exploits ZIF-67 as a self-sacrifice template for a sulfur host, CNTs as a conductive matrix and also CoS₂ sites that successfully restricted the shuttle effect [61].

Other than cobalt, other transition metals are also found to accelerate the kinetics of polysulfides redox reactions in the cathode and prevent the loss of polysulfides due to their physical and chemical interactions with them. Thus, Fe-BDC [62] and Fe-based MIL-53 [63] were used to form highly conductive honeycomb-like carbon networks enriched with Fe₃O₄ particles. In both reports, the metal oxides were found to enhance the rate capability of the prepared Li-S batteries. Liu et al. used Mn-BTC as a source of Mn molecules and spherical carbon frameworks to assemble an efficient immobilizer matrix for sulfur species as presented in Figure 4 [64]. The Mn/C-(N, O) cathode material when implemented in an in situ prepared Li-S battery exhibited durability (400 cycles at 0.2C) and increased initial capacity (1330 mAh/g at 0.2C), which were attributed to the catalytic properties of Mn species.

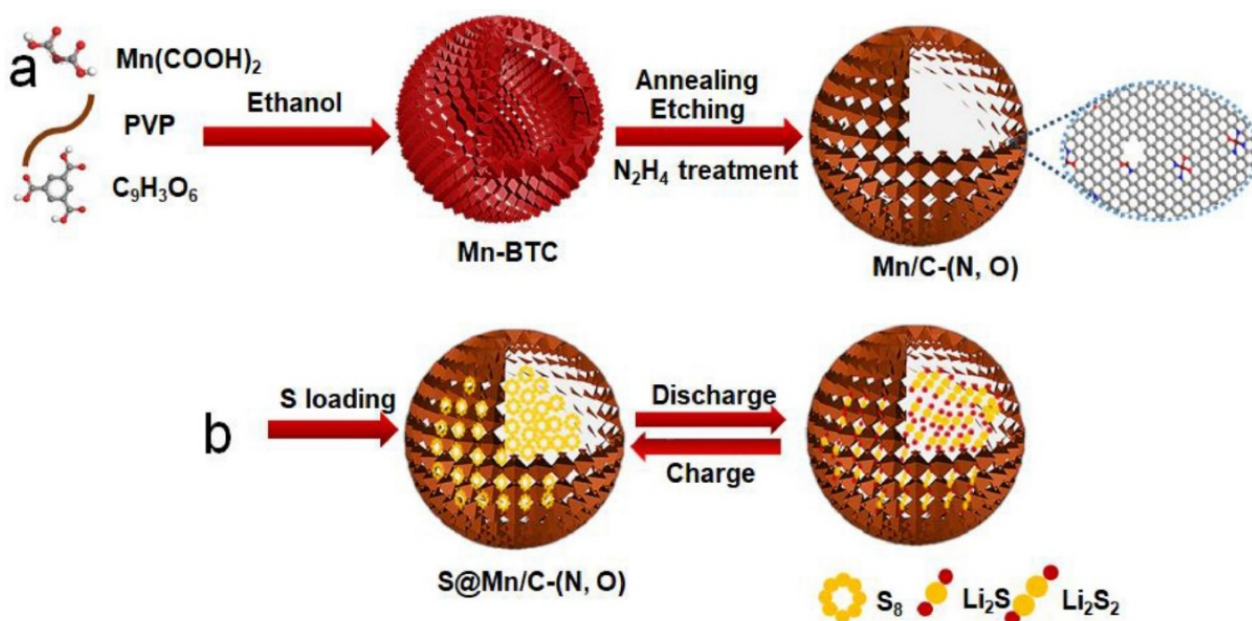


Figure 4. (a) Schematic illustration of the synthetic process for Mn/C-(N, O) and the detailed structure of Mn/C-(N, O) where Mn residues embedded in a 3D carbon framework predominantly exist as single atoms coordinated with O and N atoms, (b) Schematic illustration of the trapping mechanism of sulfur and polysulfide species in S@Mn/C-(N, O) composites. Reproduced with permissions from [64]. (Copyright 2021, Elsevier).

Similarly, selenium, belonging to the same group as sulfur, and possessing a higher electrical conductivity is recently viewed as a potential alternative for lithium battery cathodes. Selenium molecules can provoke dissolution problems if they form high order lithium selenides and could also cause destructive expansion through the cycling of the battery. Several recent articles have attempted to implement MOFs as appropriate hosts for Se active material [65].

Li et al. performed an in-situ solvothermal (under reflux) growth of Al-MIL-68 onto MWNTs (Figure 5) [66]. The collected composite had formed an interconnected web, with MOF crystals stringed through the conductive CNTs, capable of polyselenides confinement and electrolyte facilitation (Figure 3). Compared to the pure MIL-68, the composite exhibited 50% higher capacity, reaching 453 mAh/g at 0.2C after 200 cycles [66].

ZIF-8 and MOF-5 constitute some of the early proposed MOFs to be used as self-sacrifice templates to fabricate porous carbon structures and accommodate polyselenides [67,68].

Li et al. highlighted the importance of heteroatom doping when constructing porous structures to incorporate selenium. The team synthesized nitrogen-doped rod-like carbon sponges from an Al-MOF and applied them in a Li-Se battery system. The battery attained 200 galvanostatic charge/discharge cycles delivering a specific capacity of 443.2 mAh/g at 0.5C (Figure 6) [69]. Carbonization of SAF led to easily made carbon nanosheets which proved to be really durable facing Se/Li reactions preventing the whole matrix from expanding [69].

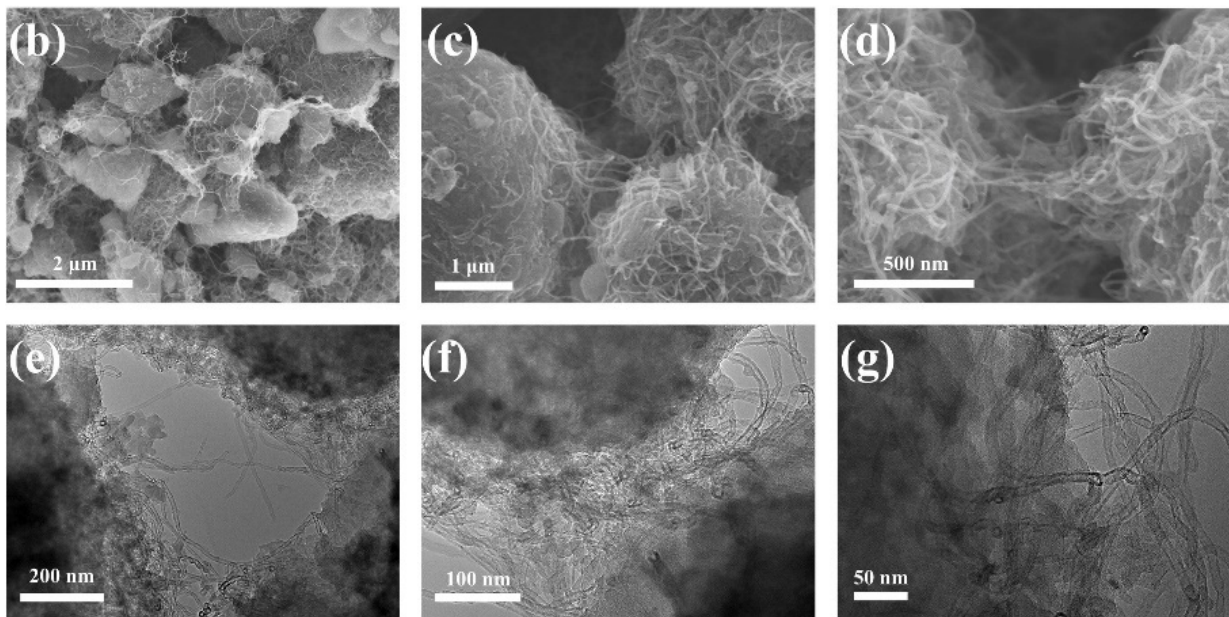
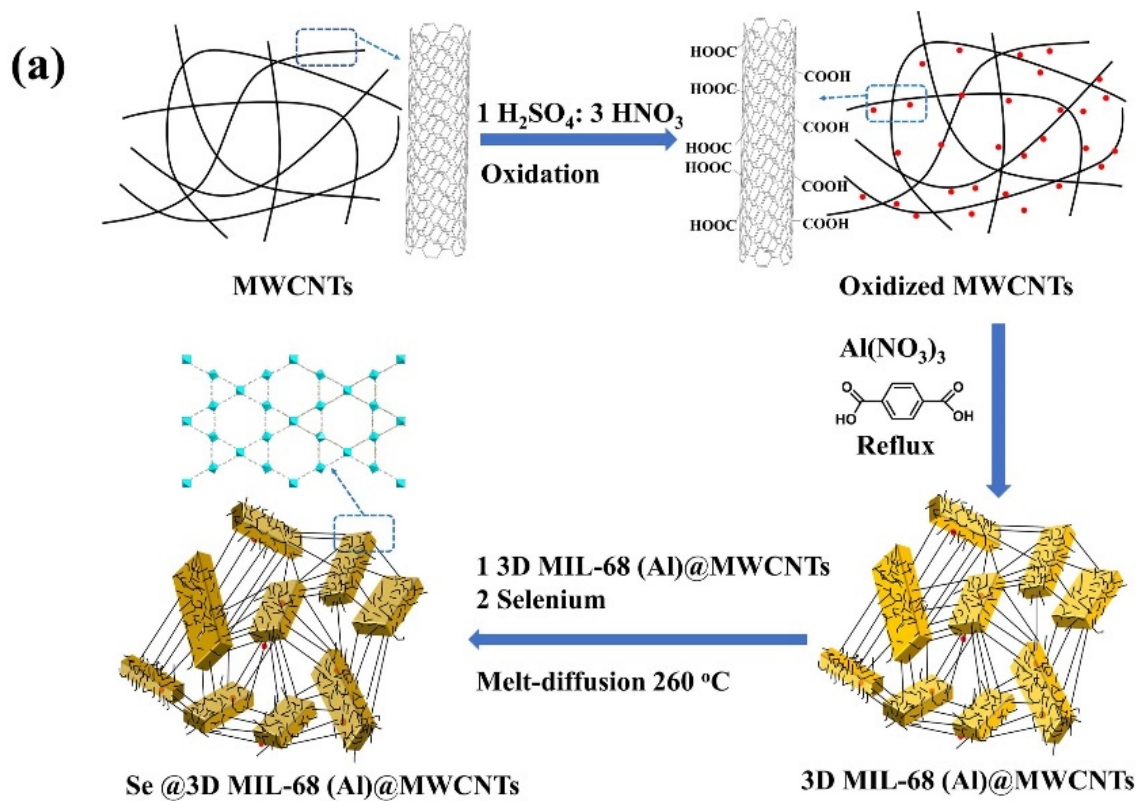


Figure 5. (a) Schematic illustration of Al-MIL-68@MWCNTs synthesis, (b–d) SEM pictures, (e–g) TEM pictures. Adapted with permissions from [66]. (Copyright 2021, Elsevier).

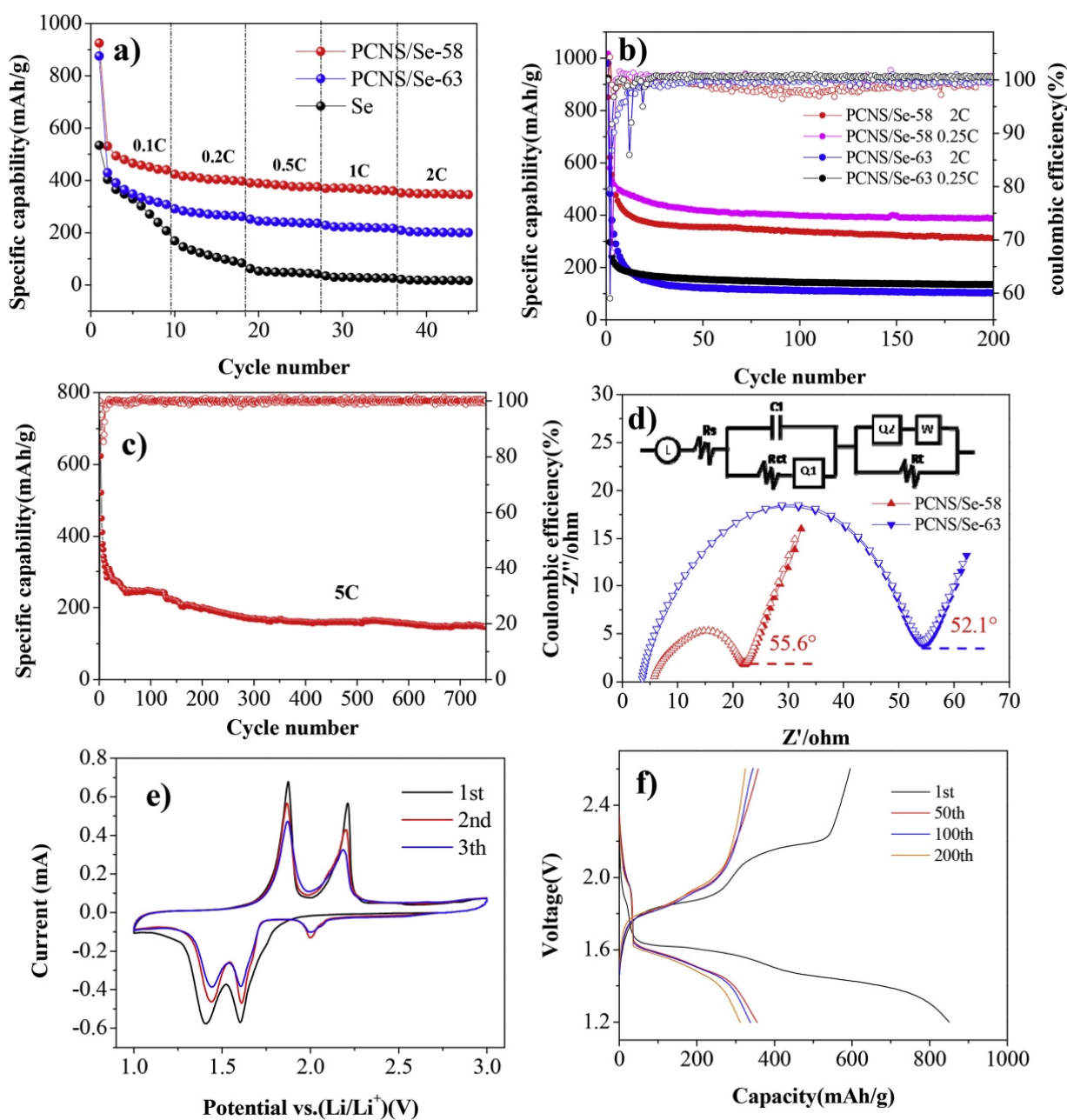


Figure 6. (a) Rate performances of PCNS/Se–58, PCNS/Se–63 and pure Se electrodes, (b) Cycle performance of PCNS/Se-58 and PCNS/Se-63 at 2C, (c) Cycle performance of PCNS/Se-58 at 5C, (d) the equivalent circuit for the battery, and solid triangle denote experimental data while the hollow triangle represents the fitted data, (e) CV curve of PCNS/Se-58 composites, (f) Discharge/charge curves of PCNS/Se-58 composites at 2C for the 1st, 50th, 100th and 200th cycle, respectively. Reproduced with permission from [69]. (Copyright Elsevier).

Park et al. investigated MOF-derived structures that combine mesopores and micropores by in situ carbonization of hybrids containing ZIF-8 deposited on other carbon structures. PAN nanofibers [70] and crumpled graphene balls (CGBs) [71] were tested as potential ZIF-7 supports and melt diffusion was conducted to complete Se loading. In the second case, the cathode material was denoted as NPC/CGB and the Li-Se battery exhibited better initial capacity (998 mAh/g versus 921 mAh/g at 0.5C) and prominent stability during continuous cycling (81.4% capacity retention at 10th cycle versus 79.2% capacity retention at 2nd cycle). Comparable battery performance results were obtained by a carbonaceous cathode prepared from a Zn/Ni-MOF2 precursor [72]. The porous carbon

microcubes (CMCs) were enriched with Se via a melt diffusion process and successfully applied in a Li-Se battery.

Apart from the most usual Li/Se [73] batteries, Li/SeS₂ have been investigated as well [74–76]. Cong et al. reported the in situ growth of ZIF-67 on graphene nanosheets (GNs) that was further annealed under Ar (650 °C) to receive Co-NC@GN and finally obtain CoP-NC@GN with the addition of phosphorous precursor (350 °C) [76]. The GNs substrate provided the expanding area of nanosized CoP and promoted electron transfer, whereas CoP active sites could chemically capture the polysulfides/selenides intermediates. The hybrid delivered an initial capacity of 868 mAh/g, which dropped to 580 mAh/g after 200 cycles at 2 A/g. The previous stage of the composite (Co-NC@GN) along with a sample without GNs (Co-NC) were also tested but with inferior results, indicating the significance of the substrate.

3. Metal Ion Batteries

The widespread use of wearable electronics has brought the need for flexible types of energy storage devices, with many efforts taking place in the field of metal-ion batteries. In Metal-Ion batteries like Li-ion, the cathode is the Li-containing electrode and is usually composed of transition metal oxides, such as LiMO₂, LiM₂O₄ and LiMPO₄ (M = Mn, Co, Ni, etc.). On the other side of the battery cell, the anode is still dominated even at the research level by graphitic carbon materials [77]. The specific capacity of the battery depends on the molecular weight of the material used in the cathode, unlike Li-S and Li-Se batteries where Lithium dominates the theoretical capacity of the battery. For instance, a LiCoO₂ cathode offers a theoretical capacity of 274 mAh/g [78] while a LiFePO₄ cathode until 160 mAh/g [79].

The first report of a MOF applied in a Li-ion battery can be found back in 2005 with MOF-177 [80]. A few years later Fe²⁺ and Fe³⁺ started being explored as redox centers in MOFs such as MIL-53 [81,82] and MIL-68 [83]. Other than their common linker, terephthalic acid, these MOFs displayed alternative structures depending on the different synthesis conditions. In fact, MIL-53 comprised of triangular shaped pores while MIL-68 hexagonal shaped pores which restricted the Li-containing electrolyte from fully diffusing into the material.

Further attention was given later to the MIL family, with Fe containing MIL-101 [84,85] which is considered to demand inexpensive materials and simple solvothermal methods to be synthesized, while the incorporation of Li atoms in the MOF is possible. The MOF was found to secure the battery from oxidation reactions of the electrolyte and attribute to the battery's thermal stability, while also being notably stable after extensive galvanostatic cycling. However, the initial discharge capacity was still relatively low when compared to conventional cathodes [85]. A higher initial specific capacity of 172 mAh/g at 50 mA/g was reached by another iron-containing MOF based on ferrocenedicarboxylate (Fe₂(DFc)₃). Moreover, the cathode could attain 10,000 cycles delivering a specific capacity of 70 mAh/g at 2000 mA/g [86].

Moving from iron-based MOFs to copper-based MOFs, a Cu-TCA (tricarboxytriphenyl amine linker) was applied in a Li-ion cell and delivered capacity retention of only 39% over 200 cycles possibly due to redox activity loss of Cu ions [87]. Later, Nagatomi et al. [88] prepared a MOF denoted as 2D Cu-CuPC based on a phthalocyanine linker and combines successfully a network of micropores (1.4 nm) and mesopores (11 nm) contributing to a BET surface area of 358 m²g⁻¹. The MOF delivers promising initial specific capacity, even comparable to conventional cathodes, however, it needs an electrical conductivity enhancement in order to be fully applicable in a LIB. Tian et al. proposed that a 2D MOF layered structure would be more favorable for Li diffusion kinetics. They synthesized a series of naphthalenediimide-based MOFs containing cadmium or cobalt metal centers via a facile room-temperature anion and thermodynamic control. Afterward, the MOFs were evaluated regarding their electrochemical properties in Li-ion coin cell type batteries. Very recently, a 3-D Co-MOF [89] and a MnCo-MOF [90] were synthesized and applied in a Li-ion

cell. The Mn-CO bimetallic MOF specifically exhibited superior catalytic activity as revealed by 600 galvanostatic cycles at 1000 mA/g and the discharge capacity of 337 mAh/g.

He et al. prepared a vanadium MOF (MIL-47) onto CNT fibers via a solvothermal method [91]. The SEM analysis revealed the critical role of reaction time, considering that decreased durations resulted in more dense/compact morphology (12 h), while increasing the reaction time to 24, 48 or even 60 h led to a fluffier framework (Figure 7). The anode was fabricated by electrodepositing zinc onto CNT fibers and the two electrodes were immersed into gel electrolyte (based on zinc chloride and PVA) and then twisted together. The assembled device presented a maximum energy density of 30.7 mWh/cm³ and a power density of 1.46 W/cm³. The flexibility was verified under different bending angles and the stability was adequate (81.5% retention after 300 cycles) to enable future research for such materials.

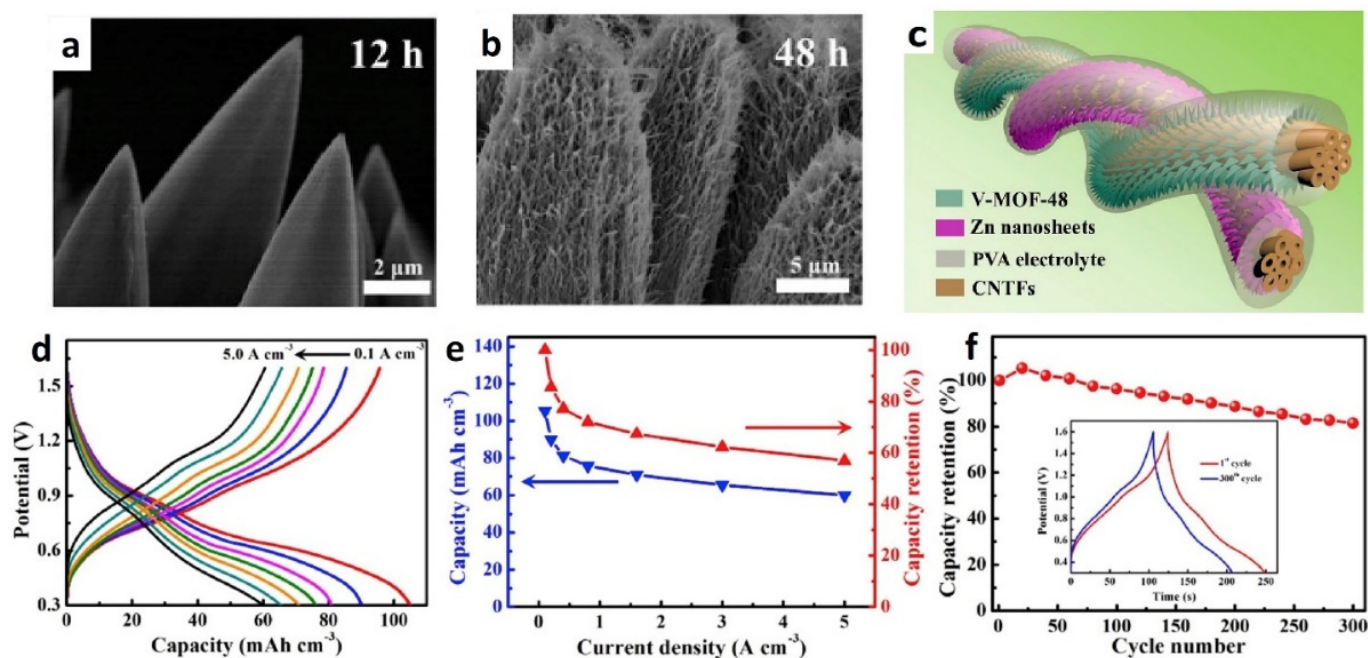


Figure 7. SEM images of V-MIL-47@CNTF after (a) 12 h (V-MOF-12) and (b) 48 h (V-MOF-48), (c) Schematic illustration, (d) GCD curves at various current densities, (e) Specific capacities at various current densities and (f) Cycling performance of the V-MOF-48//Zn battery. Adapted with permissions from [91]. (Copyright 2019, Elsevier).

Among the NCM (or NMC) materials (Nickel, Cobalt and Manganese), NCM-333 (LiNi_{1/3}Co_{1/3}Mn_{1/3}O₂) is one of the most well-studied commercial applications of Li-ion batteries [92]. In order to increase the rate capabilities and cycling stability, Li and co-workers modified this cathode by in situ coating the surface with ZIF-8 [93]. The capacity retention was doubled to 81.4% over 300 cycles at 800 mA/g, whereas the rate performance was excellent with stable specific capacities (Figure 8). EIS also verified that the ZIF-8 layer could stabilize the growth of solid-electrolyte interface film and increase the charge transfer due to its high ionic conductivity (3.16×10^{-4} S/cm). Moreover, the group investigated the battery behavior at an elevated temperature of 55 °C, discovering that the ZIF could prevent/limit the NCM erosion by the decomposition products of the electrolyte.

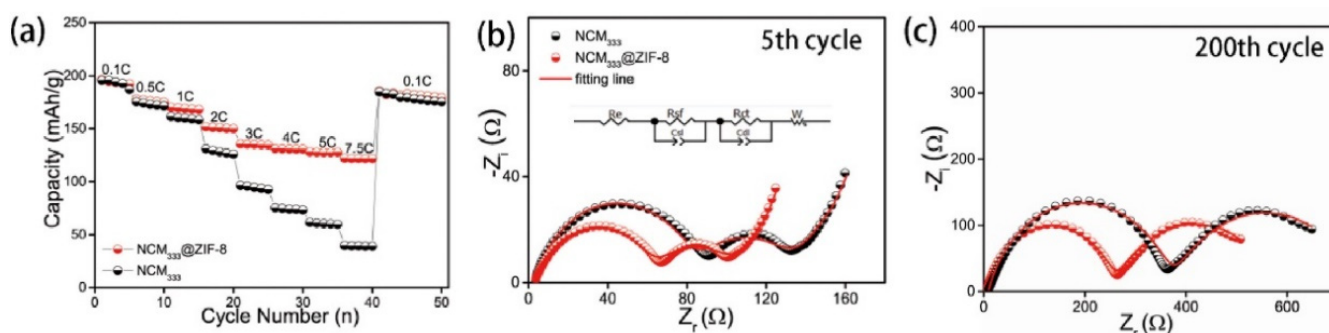


Figure 8. (a) Rate performance from 0.1C to 7.5C, Electrochemical impedance spectra during the (b) 5th cycle and (c) 200th cycle at 2C for NCM333 and NCM333@ZIF-8 electrodes. Inset of (b) is equivalent circuit. Reproduced with permissions from [93]. (Copyright 2020, Elsevier).

Monocline $\text{Li}_3\text{V}_2(\text{PO}_4)_3$ has been an attractive option in recent research for cathode materials applied in Li-Ion batteries, due to its increased potential and theoretical capacity of Li ions [94–96]. Nevertheless, this compound suffers from intrinsically low electronic conductivity, thus several composites with carbon matrixes have been explored to form more efficient cathodes. MOFs constitute accessible precursors to form various carbon architectures. ZIF-8 ($\text{Zn}(\text{MeIM})_2$) has been used as a carbon precursor, to be combined with $\text{Li}_3\text{V}_2(\text{PO}_4)_3$ by flakes and nanorods under thermal treatment in order to form a sandwich-like geometry [94]. The effect of the carbonaceous foundation attributed promising features to the constructed electrode, regarding specific capacity retention (83.2% after 2500 cycles), however, the material was not tested in an assembled Li-ion battery. According to recent research however, MIL-101(V) [95] and a V-MOF [96] can be considered a precursor for both $\text{Li}_3\text{V}_2(\text{PO}_4)_3$ and carbon frameworks. Particularly, Wang et al. proposed the use of a cathode material denoted as LVP/P-C nanocomposites that presented promising stability over 1100 cycles at a current of 10C [96].

In the same direction, MIL-47(V) was used as a precursor to synthesize both active material particles (V_2O_5) and the carbon-coated layer via a controlled thermal decomposition process [97]. The electrochemical performance of the material proved to surpass bare V_2O_5 . V_2O_5 has been also investigated as a cathode material for Li-ion batteries when stabilized on ZIF-67-derived carbon dodecahedra [98]. The aforementioned composite provides a number of advantageous features such as increased electronic and ionic conductivity, extended active surface area and homogeneous dispersion of active sites, while when synthesized at optimum conditions it can deliver an excellent specific capacity of 117.7 mAh/g at an extremely demanding current of 64C [98].

In alternative cases, MOFs can be conceived as precursors for materials, which are intended to be used as coatings around the cathode material particles, such as for $\text{Li}_{1.2}\text{Mn}_{0.54}\text{Ni}_{0.13}\text{Co}_{0.13}\text{O}_2$ [99,100]. A similar approach has been proposed in order to enhance the efficiency of anthraquinone (AQ) as a cathode material for LIBs by confining molecules inside ZIF-8-derived 3D carbon frameworks [101]. One year later the same group developed a strategy to tackle fading and instability phenomena of the cathode, by polymerization of the active material inside the carbon polyhedral (Figure 9) [102]. The cathode material denoted as PAQS@3D-C could attain a specific capacity above 200 mAh/g for 500 cycles at 0.2C.

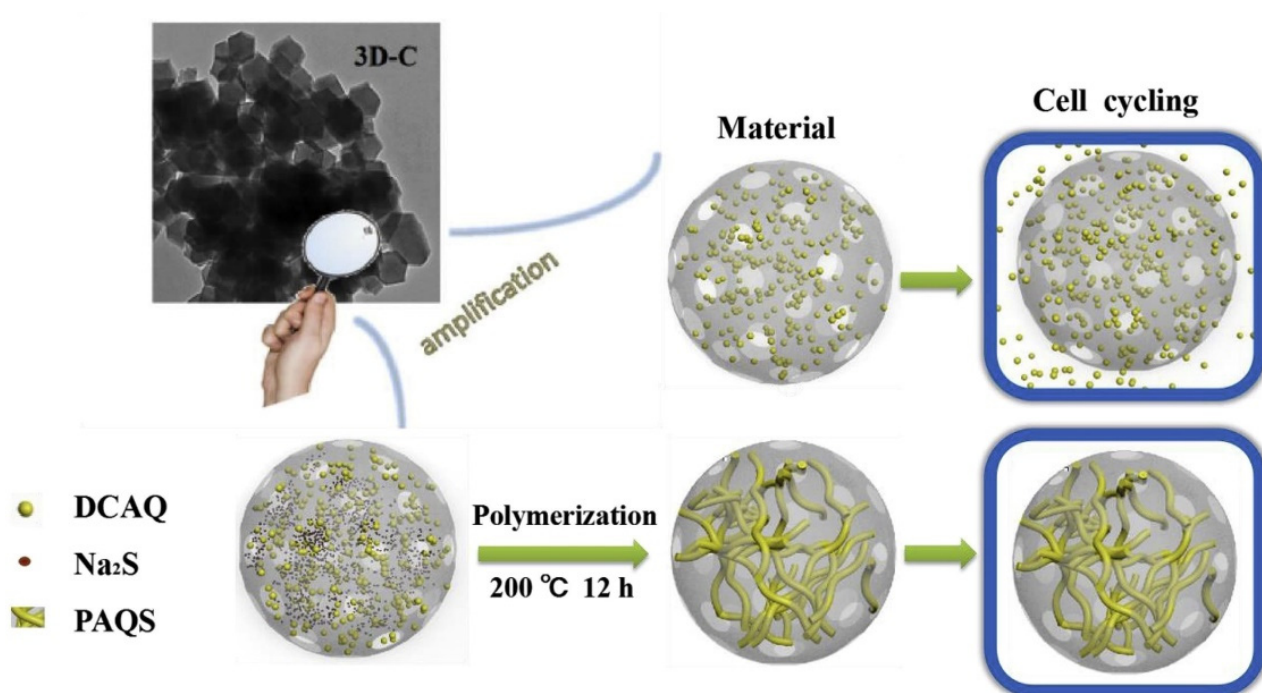


Figure 9. Synthesis process of PAQS@3D-C. Adapted with permissions from [89]. (Copyright 2020, Elsevier).

Vanadium oxides have been investigated as cathode materials also for ZIBs, thus carbon coating has been practiced for these applications too in order to boost the electronic conductivity of V₂O₅. Wang et al. constructed a novel Cu_{0.26}V₂O₅@C composite using CuBTC as both a Cu-doping source and carbon framework coating [103]. The performance of the corresponding electrode when submitted to cyclic voltammeteries and when applied in a ZIB is presented in Figure 10 [103].

ZIF-8 has been exploited to construct a honeycomb ZnO/N/C cathode material with superior characteristics and performance, regarding energy density, power density and durability when implemented in an in-situ assembled aqueous ZIB [104]. More specifically, the electrode delivered 97% of the initial capacity (114.4 mAh/g) after 8000 cycles of cycling. ZIF-8 was also used to decorate MnO_x rods with N-doped onion-like carbon leading to favorable mechanical support through volume alterations from cycling and significantly tuning the electronic and ionic conductivity of the composite [105]. Zinc ions transportation is further promoted, and the exposed active surface area is extended, thus the prepared electrode showed prominent behavior when compared to bare MnO₂ and MnO_y electrodes.

An Mn-containing MOF was firstly deposited on CNTs and subsequently thermally treated in an air atmosphere to form a hybrid denoted as MnO_x@C@CNT. The material was applied afterward as a ZIB cathode that attained 5000 cycles at 3 A/g and supplied the capacity of 95.6 mAh/g [106].

MOFs have been also considered as a source of carbon matrixes in order to immobilize active cathode species for Na-Ion battery applications. ZIF-8 derived N-doped polyhedra were used to host Poly (3,4,9,10-perylenetetracarboxylic dianhydride ethylene di-amine) (PI) to form a PI@NC composite that preserved the morphology of ZIF-8 [107]. When applied as cathode material in a SIB full cell, PI@NC demonstrated initial capacity of 101 mAh/g and a capacity retention of ~60% for 60 charge-discharge cycles at a demanding current density of 50 mA/g.

In the same direction, Lu et al. constructed a highly functional-Fe-MIL derived cathode material consisting of carbon-coated FeS₂ nanoflakes dispersed on nanorods forming sea-cucumber-like architecture [108]. This design enhances Na⁺ mobility, limits the influence of volume expansion and holds intrinsic electronic activity due to the existence of the carbon

coat. The electrode presented prominent stability over 10,000 continuous cycles at a current density of 20 A/g. Beyond typical MOF polyhedra or nanorods, Fe-MIL-derived graphitic carbon was proposed as an effective matrix to stabilize FeF₂ NPs.

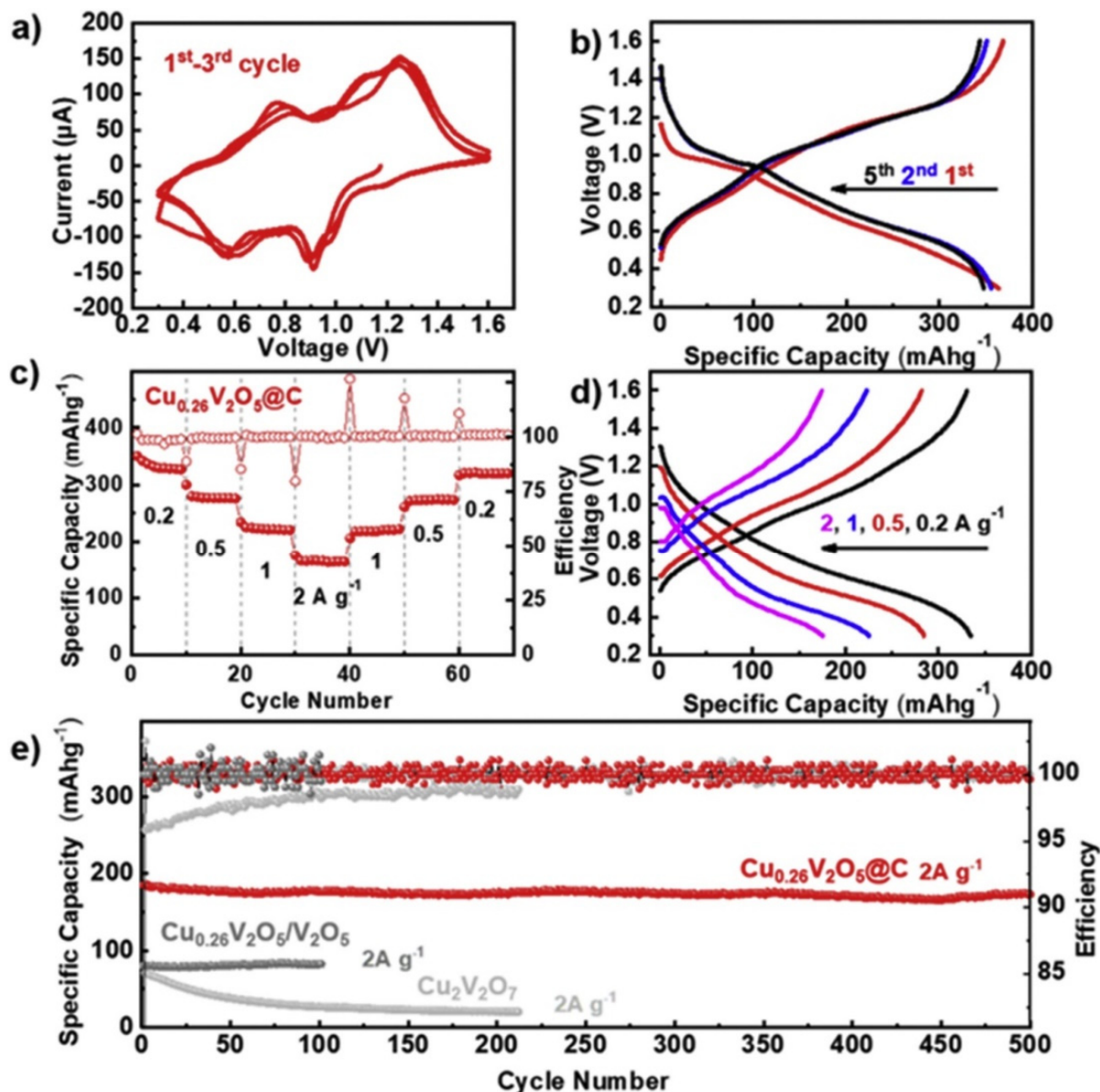


Figure 10. (a) The first three CV curves of $\text{Cu}_{0.26}\text{V}_2\text{O}_5@\text{C}$ at a scan rate of 0.2 mV/s in the voltage range of 0.3–1.6 V, (b) the initial charge/discharge curves of $\text{Cu}_{0.26}\text{V}_2\text{O}_5@\text{C}$ at the current density of 0.2 A/g, (c) the rate performances of $\text{Cu}_{0.26}\text{V}_2\text{O}_5@\text{C}$ under different current densities, (d) the relevant charge-discharge curves under different current densities and (e) the cycling performance of $\text{Cu}_{0.26}\text{V}_2\text{O}_5@\text{C}$, $\text{Cu}_{0.26}\text{V}_2\text{O}_5/\text{V}_2\text{O}_5$, and $\text{Cu}_2\text{V}_2\text{O}_7$ under high current densities. Reproduced with permissions from [103]. (Copyright 2020, Elsevier).

4. Metal-Air Batteries

Metal-Air Batteries are a type of battery system which functions differently from conventional batteries. In a MAB cell, the reductive agent comes from a typical metal anode (Zinc, Lithium, Aluminum, etc.), however, the oxidizing agent derives from ambient air which passes through the porous cathode to reach the electrolyte. The operation of the MAB offers new prospects for these types of batteries as their weight is reduced compared to conventional systems, so they give far more extended high energy density. This is the

main reason that the attention from researchers has been revived in recent years, with the vast majority of them investigating cathode materials. The reactions occurring in the cathode are Oxygen Reduction Reaction during the discharge of the battery and Oxygen Evolution Reaction during charge. The challenge is that the cathode should contain a bifunctional electrocatalyst, which can simultaneously and effectively catalyze both of the reactions [1,3,109,110].

The state-of-the-art electrocatalysts for Zinc Air Batteries (ZABs) cathodes are noble metal (Pt and IrO₂) containing electrocatalysts while recently non-precious alternatives have been proposed such as single atom catalysts [61], carbonaceous materials [111], transition metal oxides [112], metal alloys [113], sulfides [114], etc. It is proven that characteristics like micro and meso-porosity, crystal structure and interfaces of heterostructures are dominant when it comes to oxygen electrocatalysts' performance [1]. MOFs can exhibit features like versatile porosity and expanded active surface area that constitute promising candidates as oxygen electrocatalysts in MABs cathodes [6,115].

A first attempt to incorporate MOFs in Li-O₂ cathodes was introduced by Wu et al. [116] in 2014, with MOF-5, HKUST-1 and MOF-74 and metal sites of Cobalt, Magnesium and Manganese. The finest performance was reported by MOF-74 which assured open metal sites with initial specific capacities of 3630 (Co), 4560 (Mg) and 9420 mAh/g (Mn). Nevertheless, after 6 galvanostatic cycles at 200 mA/g an inevitable drop in capacity is noticed from ~5600 (N = 1) to 1300 mAh/g (N = 6). Later on, the research on MOF-74 was continued, with Co-MOF-74 by Yan et al. [117]. At that time the effect of size on NPs (nanorods) on the performance of the cell was studied. Results proved that the nanorods with a diameter of 20 nm were superior compared to those of 800 nm. The initial capacity was 11,350 mAh/g at 100 mA/g while the cathode attained 8 cycles delivering 1000 mAh/g at a current density of 250 mA/g. An interesting approach was proposed by Kim et al. [118] who synthesized MOF-74 with a MnCo bimetallic metal center (1:4 ratio). The approach was found really successful as the electrocatalyst endured 44 cycles at 200 mA/g presenting a specific capacity of 1000 mAh/g. Similarly, a Co/Zn-MOF was synthesized recently to be successfully implemented in a Li-air battery [119].

There are several studies reporting pristine MOFs combined with carbon substances in order to form electrocatalysts able to catalyze Li-O₂ redox reaction kinetics). Zhang et al. presented the synthesis of Mn-MOF-74@CNTs as the cathode of a Li-O₂ battery [120]. Based on their analysis (XPS, XPS, SEM/TEM), they observed the formation and deposition of Li₂O₂ (as a discharge product) onto the cathode surface in dry oxygen, whereas in a humid oxygen atmosphere (≥ 200 ppm moisture) LiOH crystals (flake-like) are produced, thus this hybrid is better suited as an electrode for humid oxygen conditions, considering that LiOH is less reactive and causes fewer side reactions. By increasing the moisture levels the discharge capacity increased from 1400 to 2500 mAh/g at 125 mA/g and the cycle life improved from 14 to 60 cycles. Additionally, they examined the LiOH flakes via SEM and revealed the increased size of the flakes as the discharge process proceeded. The flakes had a preference to form on MOF NPs instead of carbon surface, probably due to stronger adsorption energy of intermediates from Mn cations open metal sites or linker functional groups.

Moving to MOF-derived carbon materials MOF-5 was prepared as a precursor for a Li-O₂ battery application. The final product was a highly porous carbon network with a BET surface area of 1255 m²/g that delivered a discharge capacity of 1437 mAh/g at the first cycle. A two-step procedure was followed to synthesize the carbon network: chemical etching and carbonization [121]. Polystyrene beads were later exploited as a template to assist the thermal treatment of ZIF-8 to form a macro and microporous electrocatalyst [122]. The resulted cathode exhibited a specific capacity of 5082 mAh/g.

A number of reports investigate ZIF-67 as a template to construct cathode composite materials enhanced with metal oxide [123,124] or metal [125] active sites. A unique cage-type ZIF-8@ZIF-67 architecture was proposed firstly by Tang et al. in order to construct highly graphitic porous carbon polyhedra with interspersed Co_3O_4 NPs for battery application [126]. The catalyst denoted as GPC- Co_3O_4 combines the advantageous features of this modulated geometric structure and intrinsic activity of the transition metal oxide particles. The in-situ made Li- O_2 battery demonstrated steady discharge and charge voltage profiles (2.62–4.16 V) when cycled with a limiting capacity (500 mAh/g) for 50 cycles. In the same direction, Zhao et al. used ZIF-8@ZIF-67 as a sacrificing template to prepare catalytic carbon polyhedral enriched with Co_3O_4 and spinel NiCo_2O_4 NPs (Figure 11) [127]. The designed structure when operated as an electrocatalyst in a Li-air cell showed a promising catalytic activity (discharge capacity of 11,673 mAh/g and stable performance for 280 cycles).

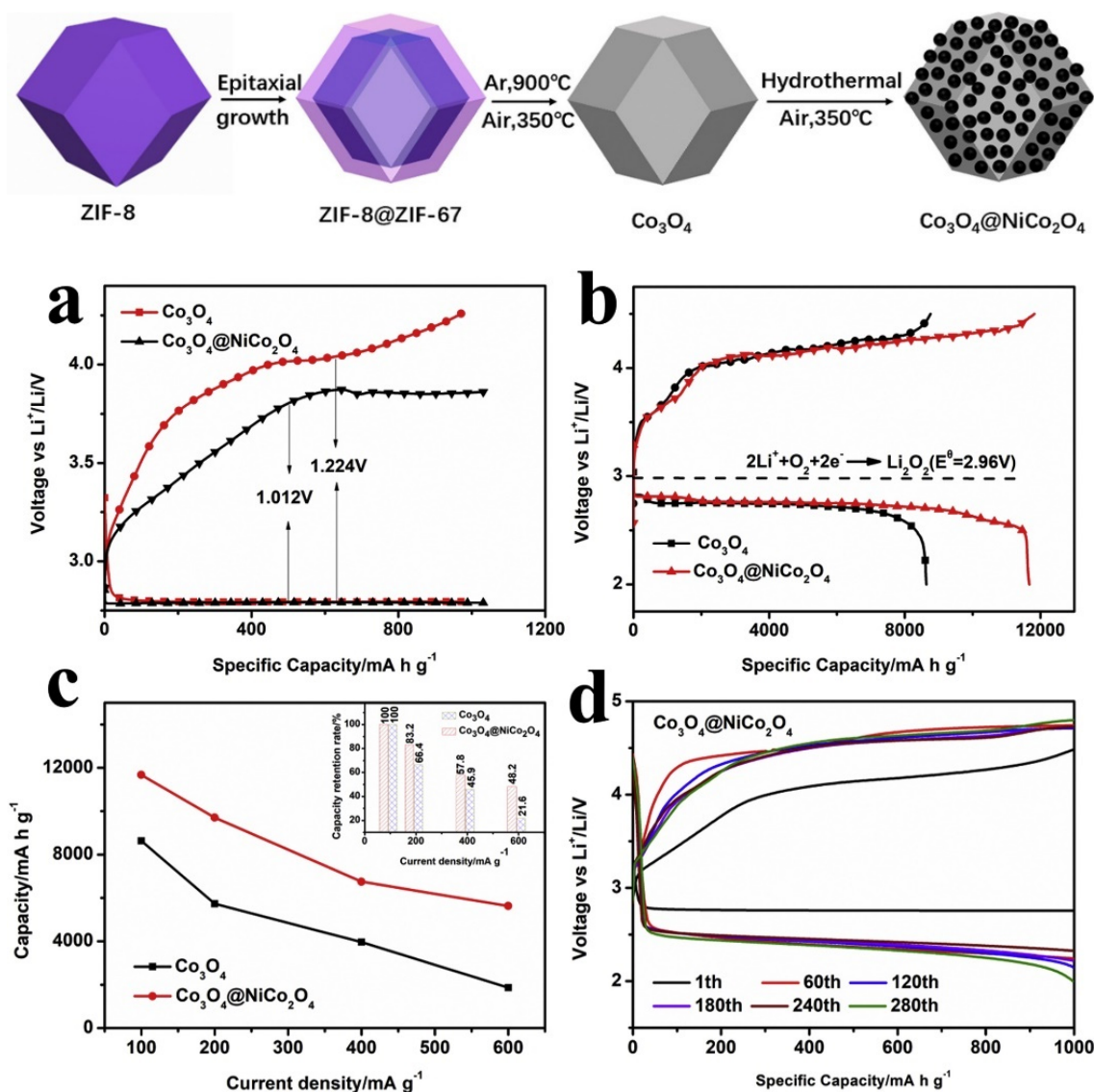


Figure 11. Top: Synthesis process of $\text{Co}_3\text{O}_4@ \text{NiCo}_2\text{O}_4$. Bottom: (a) The first charge-discharge curve of catalysts with limited capacity; (b) The first discharge-charge curves of Co_3O_4 and $\text{Co}_3\text{O}_4@ \text{NiCo}_2\text{O}_4$; (c) rate capability and capacity retention rate (inset) of Li- O_2 batteries assembled with cathodes; (d) cycling performance of $\text{Co}_3\text{O}_4@ \text{NiCo}_2\text{O}_4$ cathode. Reproduced with permissions from [127]. (Copyright 2021, Elsevier).

MIL-100 (Fe) [128] and MIL-101 (Cr) [129] have been used as precursors to construct nanocomposites with octahedral morphology and well-dispersed metal oxide active sites. These porous frameworks attribute enhanced electronic and ionic conductivity to the composite and displayed powerful properties as air cathodes in Li-O₂ batteries.

Tan et al. synthesized Co(C₄H₅N₂)₂ [Co(mIm)₂] crystals and after two-step calcination, they obtained a biphasic N-doped cobalt@graphene multiple-capsule heterostructure (BND-Co@G-MCH) [125]. DFT calculations revealed that accessible Co, CoN sites and N-doped defects on graphene can act as nucleation sites to facilitate Li₂O₂ formation.

The above cases are reported as Lithium-Oxygen Batteries, as pure oxygen is supplied instead of ambient air, so as to avoid external interventions. Li-air batteries are highly sensitive to air contaminants like CO₂ and H₂O, whose presence can cause phenomena like cracking, corrosion and pulverization. Moreover, Lithium has been reported to be explosively reactive with H₂O, consequently, much effort has been devoted to developing Zinc-Air Batteries which are considered safer [130]

Perovskites have been feasible materials as OER catalysts, due to their low cost and catalytic activity [112]. However, they suffer from the low surface area, which is crucial for such applications, hence approaches, like doping of either A or B sites have been investigated but had not been always effective, due to the low solubility of those elements [131,132]. Wang and co-workers reported the in-situ growth of Co-MOF-74 rods onto a pre-prepared LaCoO_{3-δ} perovskite [133]. Albeit LC is not a good OER electrocatalyst, the group selected it to underline the significance of the MOF/LC interface. This functionalization induced the creation of active sites due to cobalt ions from LC coordinating with the MOF ligand, thus breaking the scaling relationship of oxygen intermediates (*OH, *O, and *OOH) and reducing OER overpotential [134]. The zinc-air battery (ZAB) displayed good cycling stability over 120 h at 5 mA/cm² with a charge/discharge voltage of 2.00/1.33 V, respectively [133]. Moreover, other than the 2,5-dihydroxy-terephthalic acid, additional linkers were tested, such as trimesic acid and 2-methylimidazole, with promising results.

A combination of MOF and its carbon derivative was prepared by Huang et al. [135]. NiCo-MOF (based on 2,6-naphthalenedicarboxylic acid) was grown onto nickel foam substrate and was then annealed in an N₂ atmosphere to receive Ni-Co/C (A-NCM). Afterward, MOF was freshly regrown onto the aforementioned annealed sample, obtaining the hybrid, denoted as R-NCM. As the air cathode in a ZAB, R-NCM exhibited the best performance, compared to both initial MOF and A-NCM, when evaluated at 10 mA/cm², a fixed capacity of 17.7 mAh and charge-discharge potential gap of 0.9 V.

ZIF-8 and ZIF-67 have been dominating recent reports that refer to the conversion of MOFs into carbonaceous composites to form oxygen electrocatalysts. Heteroatom doping is a common strategy to enhance the ORR activity of carbonaceous materials [136–138], thus a uniform polyhedron network was synthesized by a NaCl-assisted carbonization of ZIF-8 and was applied in a primary alkaline ZAB. In the same direction, a silica-assisted template method was proposed to optimize exposure of graphitic N-active sites of a ZIF-8 derived material. This method contributed to the creation of a large specific surface area (254 m²/g) comprised of a macroporous framework and microporous “walls” [137]. The experimental primary ZAB endured a relatively high current density of 120 mA/cm² to fully discharge and present a specific capacity of 770 mAh/g_{Zn}, which is very close to the theoretical capacity of a zinc electrode.

In order to increase ORR/OER active sites, the addition of single metal catalytic molecules to carbon matrixes has proven to be very effective. This methodology was applied also to ZIF-8-derived electrocatalysts in order to create a Fe-N-C hierarchically porous network. An in-situ pyrolysis of Fe-ZIF led to the aforementioned Fe-N-C hybrid which was implemented in a ZAB system. Fe atoms were noticed to improve electronic conductivity of the catalyst, as well as enhance the wettability of the cathode with the electrolyte, contributing to more triple-phase boundaries and thus better ORR properties (E_{1/2} = 0.881) [139]. After special treatment ZIF-8 was a non-expensive and facile intermediate to synthesize Fe-N doped CNTs, which also perform exceptionally as ORR catalysts and

proved to be durable cathode materials for ZABs [140,141]. Ferrocene ($\text{Fe}(\text{C}_5\text{H}_5)_2$) [142] and iron carbonyl ($\text{Fe}(\text{CO})_5$) [143] have been reported as appropriate reactants to modify ZIF-8 and prepare Fe-enhanced carbon materials. In both research the fabricated cathodes outperformed precious metal Pt/C cathodes, limiting overpotentials and exhibiting high power densities ($>200 \text{ mW}/\text{cm}^2$).

Moving to the preparation of bifunctional catalysts, which can also catalyze OER kinetics, a similar Fe and N containing ZIF-8 derived catalyst was prepared by Chen et al. [144] and implemented in a secondary ZAB which attained 600 continuous galvanostatic 10-min cycles at a current density of $10 \text{ mA}/\text{cm}^2$. Moreover, the cell exhibited an excellent specific capacity ($801 \text{ mAh}/\text{g}$) and peak power density ($184 \text{ mW}/\text{cm}^2$) (Figure 12)

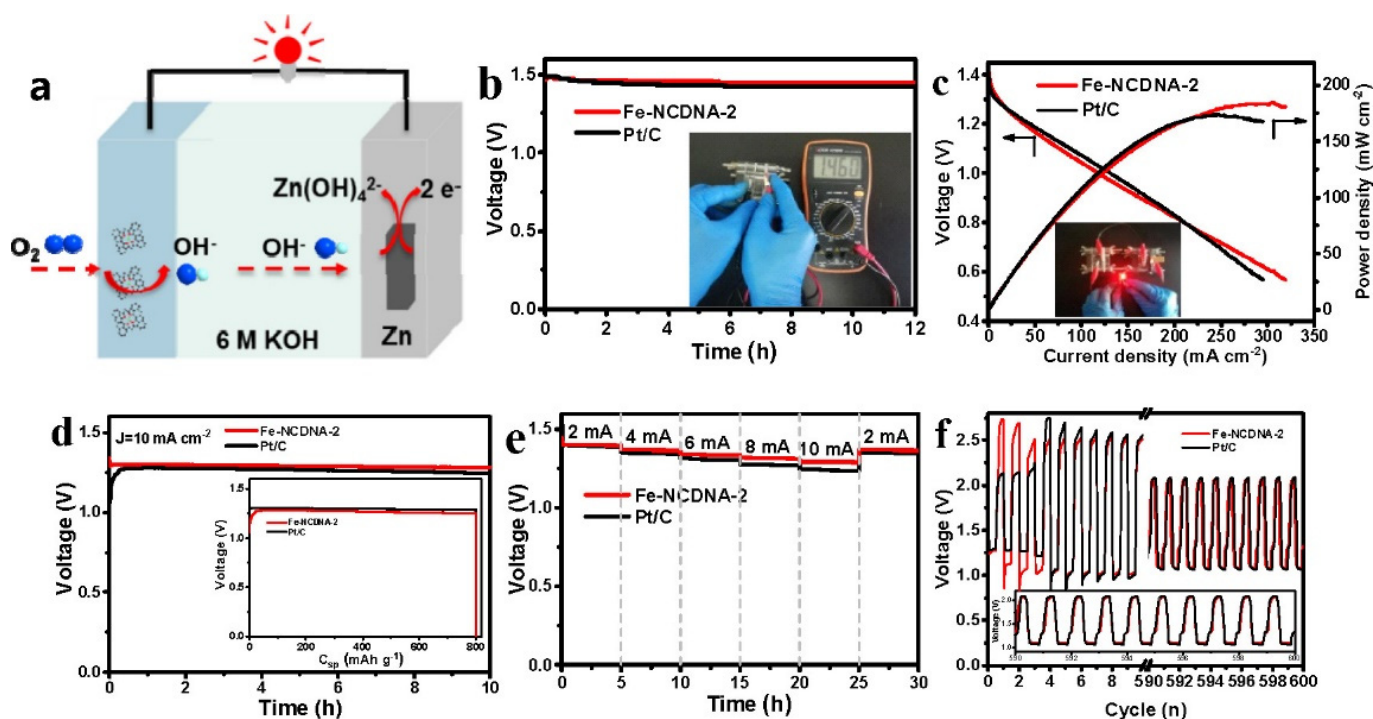


Figure 12. (a) Schematic of the home-made Zn-air battery employing Fe-NCDNA-2 as the ORR catalyst; (b) Open-circuit voltage curve; (c) Discharge polarization curves and power density. The inset shows the digital graph of a red LED powered by the constructed Zn-air battery; (d) Galvanostatic discharge curves of the Zn-air batteries with the Fe-NCDNA-2 and Pt/C as catalysts at the current density of $10 \text{ mA}/\text{cm}^2$. (Inset shows the specific capacities of the Zn-air batteries employing Fe-NCDNA-2 and Pt/C, normalized to the weight of the consumed Zn); (e) Galvanostatic discharge of the Zn-air batteries at different current densities; (f) Galvanostatic discharge–charge cycling curves at $10 \text{ mA}/\text{cm}^2$ per cycle for 10 min. Reproduced with permissions from [144]. (Copyright 2021, Elsevier).

In the same direction, cobalt has been studied regarding its properties as an ORR/OER active metal center. ZIF-67 as it contains cobalt atoms was an ideal precursor to treat in an inert atmosphere and produce a typical Co, N doped porous carbon structure (Figure 13) [145,146].

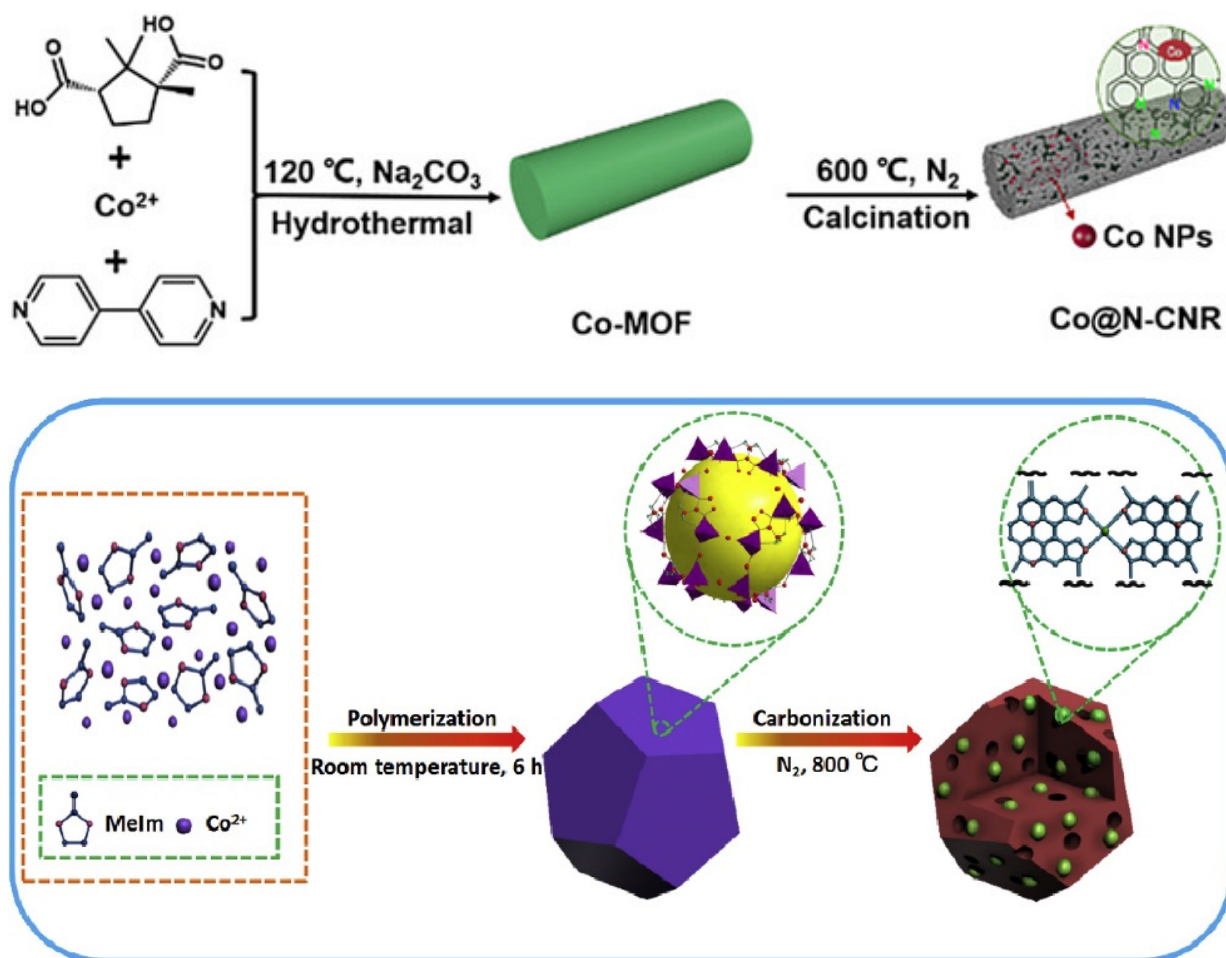


Figure 13. Top: The formation process of the Co@N-CNR catalyst. Reproduced with permissions from [145]. Bottom: The schematic illustration of the synthesis process of the Co-N-C. Reproduced with permissions from [146]. (Copyright 2018, Elsevier).

If an appropriate Co-precursor is used, Co molecules can be confined on ZIF-8 derived carbon framework and form a catalyst effective in aqueous and solid state ZABs [147]. The alkaline ZAB showed exceptional stability and endured 2-h galvanostatic cycles at the current density of 50 mA/cm^2 . The performance was attributed to the outstanding ORR and OER metrics of the electrocatalyst ($\Delta E (E_{1/2} - E_j = 10) = 0.65\text{ V}$)

Moreover, other morphologies of MOF-derived Co-N-C materials have been explored, such as nanorods [148], nanoflake arrays [149] and hexagonal structures [150].

Except for typical polyhedral carbon structures deriving from ZIF-67 or ZIF-8 frameworks, some recent studies have focused on preparing composites based on 2D layered carbon structures that can be obtained from 2D-layered ZIF (ZIF-L) sheets.

Chen et al. compared the specific surface area, pore distribution and ORR catalytic properties of cobalt decorated carbon nanostructures forming either dodecahedra (derived from ZIF-67), or nanosheets (derived from ZIF-L) [151]. Cobalt-enriched N-doped carbon nanosheets (Co-NCS) appear to possess enhanced properties, while the catalyst can be further enriched with CNTs, if Hydrogen is present in the pyrolysis process, as thoroughly explained in the article. The final product was applied in a liquid Zinc-Air Battery and strongly outperformed a state-of-art Pt electrode, with superior electrocatalytic durability (Voltage Gap $\Delta V = 0.88\text{ V}$ for 30 h of continuous cycling at a current density of 5 mA/cm^2).

Zhou et al. constructed a star-like architecture (Figure 14) based on cobalt-doped carbon structures deriving from a Co-doped ZIF-8 and ZIF-L combination [152]. The catalyst was specifically investigated towards ORR and the competent durability is attributed to the existence of Co-N₃C moieties but also to the six-nanosheet (branches) morphology which promotes the active surface area.

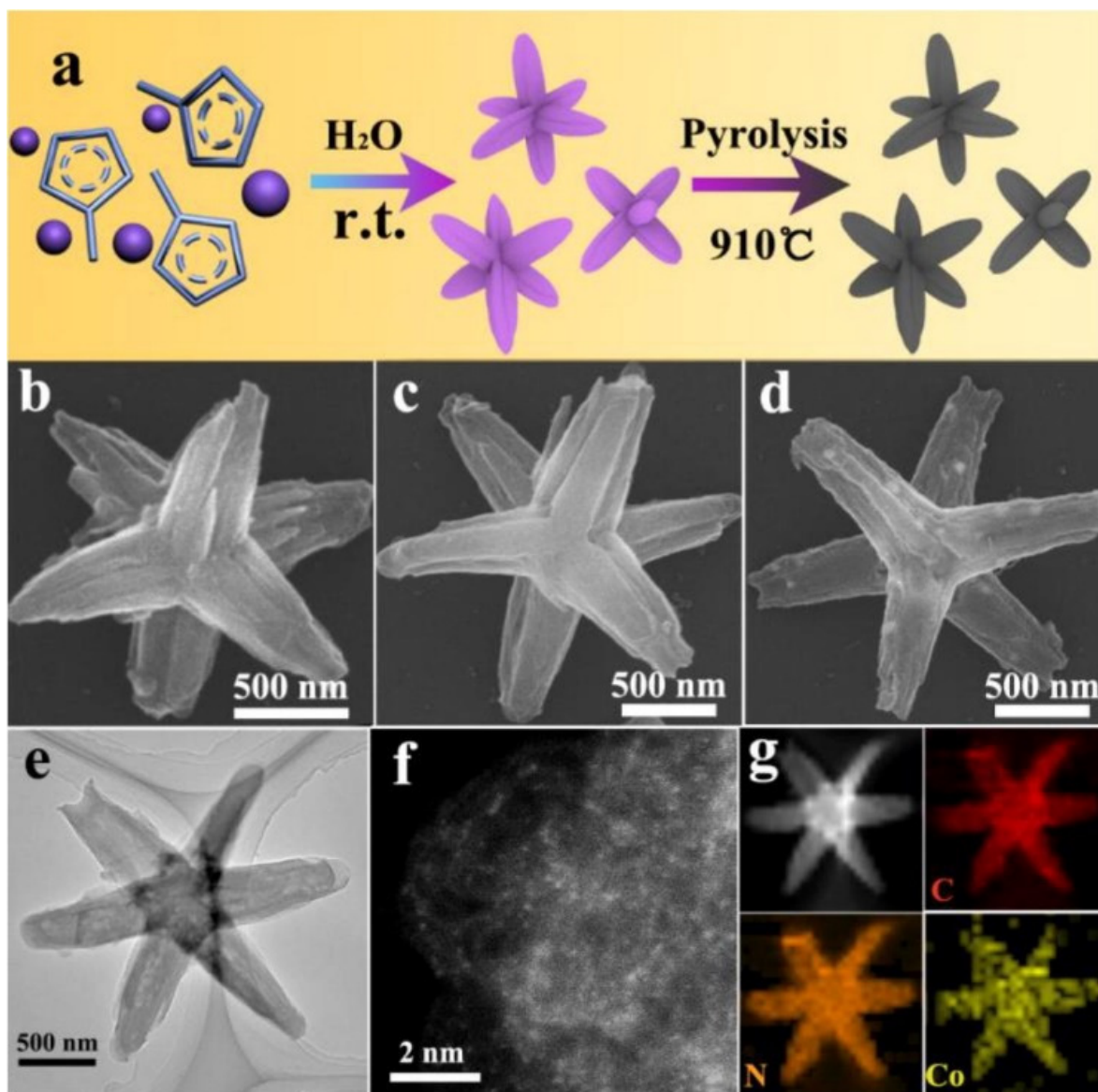


Figure 14. (a) Schematic illustration for synthesis of CoSA-N-C star-like catalysts. SEM images of (b) Co₀-N-C (no cobalt), (c) CoSA-N-C (moderate cobalt) and (d) CoNP-N-C (excessive cobalt), respectively. (e) TEM image and (f) atomic-resolution HAADF-STEM image of the CoSA-N-C. (g) The corresponding elemental mappings for the distribution of Co (yellow), C (red), and N (orange). Reproduced with permissions from [131]. (Copyright 2021, Elsevier).

Very recently Zhou et al. [153] constructed a Co/CoO decorated N,S co-doped carbon matrix via urea treatment and subsequent calcination under Argon atmosphere of a core-shell Zn-MOF@Co-MOF as shown in Figure 15. The resulted bifunctional electrocatalyst was thoroughly electrochemically investigated. It is highlighted that the catalyst outperformed the precious conventional electrode maintaining an excellent Voltage Gap of around 1 V for 400 h of galvanostatic cycling at 10 mA/cm² when applied in a liquid secondary ZAB and around 0.8 V for around 150 h of galvanostatic cycling at 10 mA/cm² when

applied in a solid-state secondary ZAB. These results were certified also by the catalyst's excellent ORR/OER properties ($\Delta E = 0.775$ V), which can be attributed to the synergistic effects of heteroatom doping, increased active surface area and open metal sites.

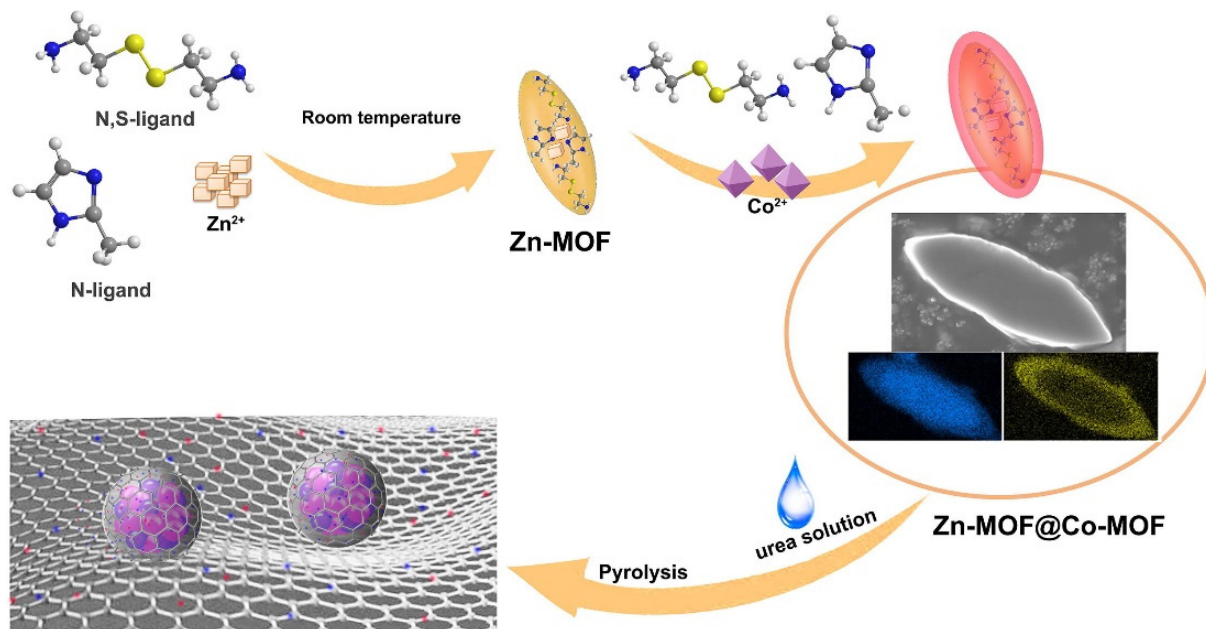


Figure 15. The schematic diagram of the synthetic pathway of Co/CoO@NSC catalysts. Reproduced with permissions from [153]. (Copyright 2021, Elsevier).

Cobalt nanoalloys such as CuCo [154] and CoFe [155] were also used to improve the catalytic properties of similar carbon leaf-like nanocomposites synthesized by thermal treatment of ZIF-L. It can be highlighted that a catalyst denoted as 2D ZnCoFe/NC was applied successfully as a cathode material in an in-situ made primary flexible battery restricting voltage overpotentials [155].

Another unique ZIF-L-based hybrid architecture was proposed in order to maximize active sites by pyrolyzing 3D MOF-on-2D MOF nano-micro arrays [156]. The catalyst denoted as ZIF-L-D-Co₃O₄/CC outperformed conventional noble electrodes regarding OER (overpotential of 310 mV to reach the current density of 10 mA/cm²) and ORR (half-wave potential $E_{1/2} = 0.9$ V). The interspersed cobalt oxide NPs multiply the active sites of the already high surface area, while the absence of a necessary binder to accomplish such a unique hierarchical structure leads to more exposed active material on the air electrode, which proved to be beneficial for the performance of the assembled ZAB.

Other than conventional MOF architectures, several studies highlight the synthesis of novel MOFs in order to modify them into bifunctional electrocatalysts for ZAB applications. Zhang et al. constructed a pair of enantiotopic chiral 3D MOFs [$Co_6(MIDPPA)_3(1,2,4\text{-btc})_3(NO_2)_3(H_2O)_3(H_2O)_7$]_n 1L and 1R, in order to explore the optimum pyrolysis temperature to obtain rod-like Co@N-C oxygen catalysts [148]. The sample denoted as C-MOF-C2-900 (pyrolysis at 900 °C) when operated as a cathode material exhibited promising ORR and OER properties, especially when observing the cycling stability of the fabricated ZAB, where the charge-discharge voltage gap is not extended more than 0.6 V for 120 h of continuous operation. In the same context, a Fe-N/C material was synthesized through direct thermal treatment of a Fe-TPP(tetraphenylporphyrin iron) ⊂ rho-ZIF (ZIF with rho topology) complex and was successfully implemented in a liquid ZAB [157].

Nanocomposites of MOF-derived materials have been tested as potential ORR electrocatalysts to be applied in primary solid state and aqueous Al-air batteries. CoNi nanoalloy particles were stabilized via a silica-assisted pyrolysis procedure into ZIF-67-derived carbon frameworks [158]. The alloys attribute to the composite dual active sites which facilitate ORR, as implied by high $E_{\text{onset}} = 1.02$ V and $E_{1/2} = 0.91$ V. Liquid and quasi-solid-state Al-Air Batteries' performance verified the prominent ORR kinetics, outperforming corresponding batteries with noble electrodes, with the liquid battery displaying a prominent peak power density of 203.69 mA/cm². ZIF-67 can be coupled with carbonaceous materials and metal compounds to be annealed in air and form nanocomposite structures with a combination of advantageous features promoting ORR. Li et al. constructed an oxygen electrocatalyst, denoted as Sm₂O₃-Co/NEC300J, which delivered 1588 mAh/g_{Al} at a discharge current density of 20 mA/cm², and a discharge voltage above 1.2 V as a cathode material [159]. The catalyst benefited from the typical polyhedral morphology derived from ZIF-67, N doping and the multiple interactions between Co and Sm₂O₃. Liu et al. prepared a coin Al-air cell enriched with a ZnO/ZnCo₂O₄/C@rGO ORR electrocatalyst which surpassed a corresponding precious metal Pt/C electrode throughout ORR polarization tests [160]. The catalyst possessed a unique structure of ZnO/ZnCo₂O₄ enhanced carbon nanocages which were dispersed into rGO nanosheets. Other than ZIF-67, a Cu-MOF was used as a precursor to form Cu/Cu₂O and amorphous CuN_xC_y species in order to enhance the catalytic properties of Ketjenblack (KB) carbon when applied in an Al-air battery [161]. The catalyst displayed prominent durability during ORR polarization tests and limited the discharging polarization of the battery (Discharge Voltage > 1.5 V) at a high current density (40 mA/cm²) when compared to a platinum catalyst.

5. Conclusions

MOFs application in energy storage systems has set the ground for further exploration of MOFs' electrochemical properties. Until now, very few reports have promising results when locating pristine MOFs in battery cathodes. On the other hand, nanocomposites with pristine MOFs offer far more possibilities by combining MOFs mainly with carbon-based materials to benefit from their electronic conductivity and the developed active interfaces.

General challenges when perceiving MOF materials as battery cathodes consist of cost and performance considerations. Realistic battery systems call for mass production of materials, avoiding as much as possible intricate and time-consuming processes. For now, the preparation of MOFs has been restricted to laboratory scale, focusing mainly on specifically enhanced characteristics of the nanoparticles, rather than simplifying the overall procedure of synthesis. Moving to restrictions regarding the performance of MOFs, it is recognized, as aforementioned, that MOFs are inferior to other electrocatalysts when it comes to electronic conductivity. Promoting electrical conductivity of such molecular frameworks has become an emerging field in recent years and some conductivity demands can be met by introducing redox active molecules or heteroatoms into the pathways of the network in order to increase internal kinetics. Alternatively, conductive polymers, carbonaceous, copper foam and nickel foam can be promising candidates to boost the electrical conductivity of MOFs. When investigating each battery system separately, high porosity is desirable, as the existence of channels favors the hostage of active materials or offers abundant reaction sites. However, such high volumes of materials inevitably will lead to a low overall volumetric energy density of the battery in future operations. This is the reason why an in-depth understanding of the mechanisms of conversion reactions or redox reactions should be conquered so we can rationally design specifically structured pores and active sites, avoiding "chasing" only the abundance of pores. The key is to completely define the relationship between the MOF structural characteristics with its electrochemical properties in a specific battery application. In this procedure, situ/operando characterization techniques should be exploited. There are cases when the properties of MOFs are dynamic and while they may play a critical role in the overall efficiency of the battery, they remain unknown.

MOF derivatives appear to meet critical demands regarding cathodes' application according to numerous reports experimenting on mainly preparing carbonaceous structures that preserve the morphology of their MOF precursor. There have been effective thermal treatment strategies for the preparation of these derivatives, exploring their resulting properties by controlling the temperature rate and gas mixtures. These derivatives are sometimes further enhanced with a metal oxide derived from the metal center of the MOF and provide a highly electronic and ionic conductive carbon porous network. Depending on the compound chosen to be associated with the mentioned network, specific advantageous electrochemical properties can be tuned in order to form hybrids with promising performance when implemented in battery cathodes.

The ongoing demand for efficient and "greener" energy storage devices has set the course for the investigation of more stable and functionalized structures to be directly implemented in such applications. Toward this end, MOFs offer broad possibilities not only due to their unique nano-morphologies and pore structure, but mostly because of their flexibility when collaborating with other substances in order to form multifunctional heterostructures.

Author Contributions: Conceptualization, C.A.; resources, G.S.; investigation, N.A., M.M., C.V. and P.K.P.; writing—original draft preparation, C.V. and M.M.; writing—review and editing, N.A., A.A.Z. and P.K.P.; supervision, C.A. and G.S. All authors have read and agreed to the published version of the manuscript.

Funding: This research received no external funding.

Institutional Review Board Statement: Not applicable.

Informed Consent Statement: Not applicable.

Data Availability Statement: Not applicable.

Conflicts of Interest: The authors declare no conflict of interest.

References

1. Mechili, M.; Vaitsis, C.; Argirusis, N.; Pandis, P.K.; Sourkouni, G.; Argirusis, C. Research progress in transition metal oxide based bifunctional electrocatalysts for aqueous electrically rechargeable zinc-air batteries. *Renew. Sustain. Energy Rev.* **2022**, *156*, 111970. [[CrossRef](#)]
2. Kwak, W.-J.; Rosy; Sharon, D.; Xia, C.; Kim, H.; Johnson, L.R.; Bruce, P.G.; Nazar, L.F.; Sun, Y.-K.; Frimer, A.A.; et al. Lithium–Oxygen Batteries and Related Systems: Potential, Status, and Future. *Chem. Rev.* **2020**, *120*, 6626–6683. [[CrossRef](#)]
3. Wang, H.-F.; Xu, Q. Materials Design for Rechargeable Metal-Air Batteries. *Matter* **2019**, *1*, 565–595. [[CrossRef](#)]
4. Gaines, L.L.; Dunn, J.B. 21-Lithium-Ion Battery Environmental Impacts. In *Lithium-Ion Batteries*; Pistoia, G., Ed.; Elsevier: Amsterdam, The Netherlands, 2014; pp. 483–508.
5. Arinicheva, Y.; Wolff, M.; Lobe, S.; Dellen, C.; Fattakhova-Rohlfing, D.; Guillon, O.; Böhm, D.; Zoller, F.; Schmuch, R.; Li, J.; et al. 10-Ceramics for electrochemical storage. In *Advanced Ceramics for Energy Conversion and Storage*; Guillon, O., Ed.; Elsevier: Amsterdam, The Netherlands, 2020; pp. 549–709.
6. Vaitsis, C.; Kanellou, E.; Angelara, C.; Pandis, P.K.; Argirusis, N.; Sourkouni, G.; Zorpas, A.A.; Karantonis, A.; Argirusis, C. Chapter 18-MOFs–metal oxides/sulfides/phosphides nanocomposites for supercapacitors. In *Metal–Organic Framework-Based Nanomaterials for Energy Conversion and Storage*; Gupta, R.K., Nguyen, T.A., Yasin, G., Eds.; Elsevier: Amsterdam, The Netherlands, 2022; pp. 393–412.
7. Vaitsis, C.; Sourkouni, G.; Argirusis, C. Metal Organic Frameworks (MOFs) and ultrasound: A review. *Ultrason. Sonochem.* **2019**, *52*, 106–119. [[CrossRef](#)] [[PubMed](#)]
8. Vaitsis, C.; Mechili, M.; Argirusis, N.; Kanellou, E.; Pandis, P.K.; Sourkouni, G.; Zorpas, A.; Argirusis, C. Ultrasound-Assisted Preparation Methods of Nanoparticles for Energy-Related Applications. In *Nanotechnology and the Environment*; IntechOpen: Rijeka, Croatia, 2020; pp. 77–103.
9. Talin, A.A.; Centrone, A.; Ford, A.C.; Foster, M.E.; Stavila, V.; Haney, P.; Kinney, R.A.; Szalai, V.; El Gabaly, F.; Yoon, H.P.; et al. Tunable electrical conductivity in metal-organic framework thin-film devices. *Science* **2014**, *343*, 66–69. [[CrossRef](#)] [[PubMed](#)]
10. Rubio-Giménez, V.; Tatay, S.; Martí-Gastaldo, C. Electrical conductivity and magnetic bistability in metal–organic frameworks and coordination polymers: Charge transport and spin crossover at the nanoscale. *Chem. Soc. Rev.* **2020**, *49*, 5601–5638. [[CrossRef](#)] [[PubMed](#)]

11. Tan, Y.; Zhu, W.; Zhang, Z.; Wu, W.; Chen, R.; Mu, S.; Lv, H.; Cheng, N. Electronic tuning of confined sub-nanometer cobalt oxide clusters boosting oxygen catalysis and rechargeable Zn–air batteries. *Nano Energy* **2021**, *83*, 105813. [[CrossRef](#)]
12. Wild, M.; O'Neill, L.; Zhang, T.; Purkayastha, R.; Minton, G.; Marinescu, M.; Offer, G.J. Lithium sulfur batteries, a mechanistic review. *Energy Environ. Sci.* **2015**, *8*, 3477–3494. [[CrossRef](#)]
13. Ren, W.; Ma, W.; Zhang, S.; Tang, B. Recent advances in shuttle effect inhibition for lithium sulfur batteries. *Energy Storage Mater.* **2019**, *23*, 707–732. [[CrossRef](#)]
14. Deng, W.; Phung, J.; Li, G.; Wang, X. Realizing high-performance lithium-sulfur batteries via rational design and engineering strategies. *Nano Energy* **2021**, *82*, 105761. [[CrossRef](#)]
15. Liu, T.; Hu, H.; Ding, X.; Yuan, H.; Jin, C.; Nai, J.; Liu, Y.; Wang, Y.; Wan, Y.; Tao, X. 12 years roadmap of the sulfur cathode for lithium sulfur batteries (2009–2020). *Energy Storage Mater.* **2020**, *30*, 346–366. [[CrossRef](#)]
16. Eftekhari, A.; Ramanujam, B. In pursuit of catalytic cathodes for lithium–oxygen batteries. *J. Mater. Chem. A* **2017**, *5*, 7710–7731. [[CrossRef](#)]
17. Vaitsis, C.; Mechili, M.; Argirusis, N.; Pandis, P.K.; Sourkouni, G.; Argirusis, C. Chapter 10-MOF nanomaterials for battery cathodes. In *Metal-Organic Framework-Based Nanomaterials for Energy Conversion and Storage*; Gupta, R.K., Nguyen, T.A., Yasin, G., Eds.; Elsevier: Amsterdam, The Netherlands, 2022; pp. 207–226.
18. Demir-Cakan, R.; Morcrette, M.; Nouar, F.; Davoisne, C.; Devic, T.; Gonbeau, D.; Dominko, R.; Serre, C.; Férey, G.; Tarascon, J.-M. Cathode Composites for Li–S Batteries via the Use of Oxygenated Porous Architectures. *J. Am. Chem. Soc.* **2011**, *133*, 16154–16160. [[CrossRef](#)]
19. Hou, Y.; Mao, H.; Xu, L. MIL-100(V) and MIL-100(V)/rGO with various valence states of vanadium ions as sulfur cathode hosts for lithium-sulfur batteries. *Nano Res.* **2017**, *10*, 344–353. [[CrossRef](#)]
20. Baumann, A.E.; Aversa, G.E.; Roy, A.; Falk, M.L.; Bedford, N.M.; Thoi, V.S. Promoting sulfur adsorption using surface Cu sites in metal-organic frameworks for lithium sulfur batteries. *J. Mater. Chem. A* **2018**, *6*, 4811–4821. [[CrossRef](#)]
21. Zhou, J.; Yu, X.; Fan, X.; Wang, X.; Li, H.; Zhang, Y.; Li, W.; Zheng, J.; Wang, B.; Li, X. Impact of the particle size of a metal-organic framework for sulfur storage in Li-S batteries. *J. Mater. Chem. A* **2015**, *3*, 8272–8275. [[CrossRef](#)]
22. Geng, P.; Wang, L.; Du, M.; Bai, Y.; Li, W.; Liu, Y.; Chen, S.; Braunstein, P.; Xu, Q.; Pang, H. MIL-96-Al for Li–S Batteries: Shape or Size? *Adv. Mater.* **2022**, *34*, 2107836. [[CrossRef](#)]
23. Cui, G.; Li, G.; Luo, D.; Zhang, Y.; Zhao, Y.; Wang, D.; Wang, J.; Zhang, Z.; Wang, X.; Chen, Z. Three-dimensionally ordered macro-microporous metal organic frameworks with strong sulfur immobilization and catalyzation for high-performance lithium-sulfur batteries. *Nano Energy* **2020**, *72*, 104685. [[CrossRef](#)]
24. Wang, T.; Liu, Y.; Liu, X.; Cui, G.; Zhang, Y.; Wang, X. Three-dimensionally Ordered Macro-porous Metal-organic Framework for High-performance Lithium-sulfur Battery. *ChemElectroChem* **2022**, *9*, e202101099. [[CrossRef](#)]
25. Liu, X.-W.; Sun, T.-J.; Hu, J.-L.; Wang, S.-D. Composites of metal-organic frameworks and carbon-based materials: Preparations, functionalities and applications. *J. Mater. Chem. A* **2016**, *4*, 3584–3616. [[CrossRef](#)]
26. Wang, J.; Gao, L.; Zhao, J.; Zheng, J.; Wang, J.; Huang, J. A facile in-situ synthesis of ZIF-8 nanoparticles anchored on reduced graphene oxide as a sulfur host for Li-S batteries. *Mater. Res. Bull.* **2021**, *133*, 111061. [[CrossRef](#)]
27. Wu, Z.; Wang, L.; Chen, S.; Zhu, X.; Deng, Q.; Wang, J.; Zeng, Z.; Deng, S. Facile and low-temperature strategy to prepare hollow ZIF-8/CNT polyhedrons as high-performance lithium-sulfur cathodes. *Chem. Eng. J.* **2021**, *404*, 126579. [[CrossRef](#)]
28. Ge, X.; Li, C.; Li, Z.; Yin, L. Tannic acid tuned metal-organic framework as a high-efficiency chemical anchor of polysulfide for lithium-sulfur batteries. *Electrochim. Acta* **2018**, *281*, 700–709. [[CrossRef](#)]
29. Bao, W.; Zhang, Z.; Qu, Y.; Zhou, C.; Wang, X.; Li, J. Confine sulfur in mesoporous metal-organic framework @ reduced graphene oxide for lithium sulfur battery. *J. Alloys Compd.* **2014**, *582*, 334–340. [[CrossRef](#)]
30. Xu, G.; Ding, B.; Shen, L.; Nie, P.; Han, J.; Zhang, X. Sulfur embedded in metal organic framework-derived hierarchically porous carbon nanoplates for high performance lithium-sulfur battery. *J. Mater. Chem. A* **2013**, *1*, 4490–4496. [[CrossRef](#)]
31. Yao, J.; Zhang, M.; Han, G.; Wang, X.; Wang, Z.; Wang, J. Reduced graphene oxide coated Fe-soc as a cathode material for high-performance lithium-sulfur batteries. *Ceram. Int.* **2020**, *46*, 24155–24161. [[CrossRef](#)]
32. Li, Z.; Li, C.; Ge, X.; Ma, J.; Zhang, Z.; Li, Q.; Wang, C.; Yin, L. Reduced graphene oxide wrapped MOFs-derived cobalt-doped porous carbon polyhedrons as sulfur immobilizers as cathodes for high performance lithium sulfur batteries. *Nano Energy* **2016**, *23*, 15–26. [[CrossRef](#)]
33. Xu, G.; Zuo, Y.; Huang, B. Metal-organic framework-74-Ni/carbon nanotube composite as sulfur host for high performance lithium-sulfur batteries. *J. Electroanal. Chem.* **2018**, *830*, 43–49. [[CrossRef](#)]
34. Pu, Y.; Wu, W.; Liu, J.; Liu, T.; Ding, F.; Zhang, J.; Tang, Z. A defective MOF architecture threaded by interlaced carbon nanotubes for high-cycling lithium-sulfur batteries. *RSC Adv.* **2018**, *8*, 18604–18612. [[CrossRef](#)]
35. Jiang, H.L.; Feng, D.; Liu, T.F.; Li, J.R.; Zhou, H.C. Pore surface engineering with controlled loadings of functional groups via click chemistry in highly stable metal-organic frameworks. *J. Am. Chem. Soc.* **2012**, *134*, 14690–14693. [[CrossRef](#)]
36. Wu, H.; Chua, Y.S.; Krungleviciute, V.; Tyagi, M.; Chen, P.; Yildirim, T.; Zhou, W. Unusual and highly tunable missing-linker defects in zirconium metal-organic framework UiO-66 and their important effects on gas adsorption. *J. Am. Chem. Soc.* **2013**, *135*, 10525–10532. [[CrossRef](#)] [[PubMed](#)]

37. Ling, S.; Slater, B. Dynamic acidity in defective UiO-66. *Chem. Sci.* **2016**, *7*, 4706–4712. [[CrossRef](#)]
38. Ji, X.; Li, Q.; Yu, H.; Hu, X.; Luo, Y.; Li, B. Three-dimensional ordered macroporous ZIF-8 nanoparticle-derived nitrogen-doped hierarchical porous carbons for high-performance lithium–sulfur batteries. *RSC Adv.* **2020**, *10*, 41983–41992. [[CrossRef](#)] [[PubMed](#)]
39. Zhang, J.; Huang, M.; Xi, B.; Mi, K.; Yuan, A.; Xiong, S. Systematic Study of Effect on Enhancing Specific Capacity and Electrochemical Behaviors of Lithium-Sulfur Batteries. *Adv. Energy Mater.* **2018**, *8*, 1701330. [[CrossRef](#)]
40. Li, X.; Sun, Q.; Liu, J.; Xiao, B.; Li, R.; Sun, X. Tunable porous structure of metal organic framework derived carbon and the application in lithium–sulfur batteries. *J. Power Sources* **2016**, *302*, 174–179. [[CrossRef](#)]
41. Li, Z.; Yin, L. Nitrogen-doped MOF-derived micropores carbon as immobilizer for small sulfur molecules as a cathode for lithium sulfur batteries with excellent electrochemical performance. *ACS Appl. Mater. Interfaces* **2015**, *7*, 4029–4038. [[CrossRef](#)] [[PubMed](#)]
42. Jiang, Y.; Liu, H.; Tan, X.; Guo, L.; Zhang, J.; Liu, S.; Guo, Y.; Zhang, J.; Wang, H.; Chu, W. Monoclinic ZIF-8 Nanosheet-Derived 2D Carbon Nanosheets as Sulfur Immobilizer for High-Performance Lithium Sulfur Batteries. *ACS Appl. Mater. Interfaces* **2017**, *9*, 25239–25249. [[CrossRef](#)]
43. Chen, R.; Zhao, T.; Tian, T.; Cao, S.; Coxon, P.R.; Xi, K.; Fairen-Jimenez, D.; Vasant Kumar, R.; Cheetham, A.K. Graphene-wrapped sulfur/metal organic framework-derived microporous carbon composite for lithium sulfur batteries. *APL Mater.* **2014**, *2*, 124109. [[CrossRef](#)]
44. Song, R.-S.; Wang, B.; Ruan, T.-T.; Wang, L.; Luo, H.; Wang, F.; Gao, T.-T.; Wang, D.-L. A three-dimensional cathode matrix with bi-confinement effect of polysulfide for lithium-sulfur battery. *Appl. Surf. Sci.* **2018**, *427*, 396–404. [[CrossRef](#)]
45. Tan, Y.; Jia, Z.; Lou, P.; Cui, Z.; Guo, X. Self-assembly sandwiches of reduced graphene oxide layers with zeolitic-imidazolate-frameworks-derived mesoporous carbons as polysulfides reservoirs for lithium-sulfur batteries. *J. Power Sources* **2017**, *341*, 68–74. [[CrossRef](#)]
46. Chen, K.; Sun, Z.; Fang, R.; Shi, Y.; Cheng, H.-M.; Li, F. Metal-Organic Frameworks (MOFs)-Derived Nitrogen-Doped Porous Carbon Anchored on Graphene with Multifunctional Effects for Lithium-Sulfur Batteries. *Adv. Funct. Mater.* **2018**, *28*, 1707592. [[CrossRef](#)]
47. Yao, Y.; Liu, P.; Zhang, Q.; Zeng, S.; Chen, S.; Zou, G.; Zou, J.; Zeng, X.; Li, X. Nitrogen-doped micropores binder-free carbon-sulphur composites as the cathode for long-life lithium-sulphur batteries. *Mater. Lett.* **2018**, *231*, 159–162. [[CrossRef](#)]
48. Bao, W.; Su, D.; Zhang, W.; Guo, X.; Wang, G. 3D Metal Carbide@Mesoporous Carbon Hybrid Architecture as a New Polysulfide Reservoir for Lithium-Sulfur Batteries. *Adv. Funct. Mater.* **2016**, *26*, 8746–8756. [[CrossRef](#)]
49. Bao, W.; Zhang, Z.; Chen, W.; Zhou, C.; Lai, Y.; Li, J. Facile synthesis of graphene oxide @ mesoporous carbon hybrid nanocomposites for lithium sulfur battery. *Electrochim. Acta* **2014**, *127*, 342–348. [[CrossRef](#)]
50. Wang, Y.; Wu, Y.; Xie, J.; Ge, H.; Hu, X. Multi-walled carbon nanotubes and metal-organic framework nanocomposites as novel hybrid electrode materials for the determination of nano-molar levels of lead in a lab-on-valve format. *Analyst* **2013**, *138*, 5113–5120. [[CrossRef](#)]
51. Zhou, J.; Lin, N.; long Cai, W.; Guo, C.; Zhang, K.; Zhou, J.; Zhu, Y.; Qian, Y. Synthesis of S/CoS₂ Nanoparticles-Embedded N-doped Carbon Polyhedrons from Polyhedrons ZIF-67 and their Properties in Lithium-Sulfur Batteries. *Electrochim. Acta* **2016**, *218*, 243–251. [[CrossRef](#)]
52. Luo, S.; Zheng, C.; Sun, W.; Wang, Y.; Ke, J.; Guo, Q.; Liu, S.; Hong, X.; Li, Y.; Xie, W. Multi-functional CoS₂-N-C porous carbon composite derived from metal-organic frameworks for high performance lithium-sulfur batteries. *Electrochim. Acta* **2018**, *289*, 94–103. [[CrossRef](#)]
53. Gao, H.; Ning, S.; Zhou, Y.; Men, S.; Kang, X. Polyacrylonitrile-induced formation of core-shell carbon nanocages: Enhanced redox kinetics towards polysulfides by confined catalysis in Li-S batteries. *Chem. Eng. J.* **2021**, *408*, 127323. [[CrossRef](#)]
54. He, J.; Chen, Y.; Lv, W.; Wen, K.; Xu, C.; Zhang, W.; Li, Y.; Qin, W.; He, W. From Metal-Organic Framework to Li₂S@C-Co-N Nanoporous Architecture: A High-Capacity Cathode for Lithium-Sulfur Batteries. *ACS Nano* **2016**, *10*, 10981–10987. [[CrossRef](#)] [[PubMed](#)]
55. Song, Z.; Lu, X.; Li, X.; Jiang, N.; Huo, Y.; Zheng, Q.; Lin, D. Tailored multifunctional hybrid cathode substrate configured with carbon nanotube-modified polar Co(PO₃)₂/CoP nanoparticles embedded nitrogen-doped porous-shell carbon polyhedron for high-performance lithium-sulfur batteries. *J. Colloid Interface Sci.* **2020**, *575*, 220–230. [[CrossRef](#)]
56. Li, M.; Feng, W.; Wang, X. The dual-play of carbon nanotube embedded with CoNi N codoped porous polyhedra toward superior Lithium–Sulfur batteries. *J. Alloys Compd.* **2021**, *853*, 157194. [[CrossRef](#)]
57. Lu, H.; Zhang, C.; Zhang, Y.; Huang, Y.; Liu, M.; Liu, T. Simultaneous growth of carbon nanotubes on inner/outer surfaces of porous polyhedra: Advanced sulfur hosts for lithium-sulfur batteries. *Nano Res.* **2018**, *11*, 6155–6166. [[CrossRef](#)]
58. Zhu, Y.; Zheng, H.; Cen, J.; Ali, A.; Chen, X.; Shen, P.K. High performance lithium-sulfur batteries based on CoP nanoparticle-embedded nitrogen-doped carbon nanotube hollow polyhedra. *J. Electroanal. Chem.* **2021**, *885*, 114996. [[CrossRef](#)]
59. Xu, F.; Dong, C.; Jin, B.; Li, H.; Wen, Z.; Jiang, Q. MOF-derived LDH wrapped with rGO as an efficient sulfur host for lithium-sulfur batteries. *J. Electroanal. Chem.* **2020**, *876*, 114545. [[CrossRef](#)]
60. Wan, T.; Liu, S.; Wu, C.; Tan, Z.; Lin, S.; Zhang, X.; Zhang, Z.; Liu, G. Rational design of Co nano-dots embedded three-dimensional graphene gel as multifunctional sulfur cathode for fast sulfur conversion kinetics. *J. Energy Chem.* **2021**, *56*, 132–140. [[CrossRef](#)]
61. Chen, C.-H.; Lin, S.-H.; Wu, Y.-J.; Su, J.-T.; Cheng, C.-C.; Cheng, P.-Y.; Ting, Y.-C.; Lu, S.-Y. MOF-derived cobalt Disulfide/Nitrogen-doped carbon composite polyhedrons linked with Multi-walled carbon nanotubes as sulfur hosts for Lithium-Sulfur batteries. *Chem. Eng. J.* **2022**, *431*, 133924. [[CrossRef](#)]

62. Fan, L.; Wu, H.; Wu, X.; Wang, M.; Cheng, J.; Zhang, N.; Feng, Y.; Sun, K. Fe-MOF derived jujube pit like Fe₃O₄/C composite as sulfur host for lithium-sulfur battery. *Electrochim. Acta* **2019**, *295*, 444–451. [[CrossRef](#)]
63. Liu, G.; Feng, K.; Cui, H.; Li, J.; Liu, Y.; Wang, M. MOF derived in-situ carbon-encapsulated Fe₃O₄@C to mediate polysulfides redox for ultrastable Lithium-sulfur batteries. *Chem. Eng. J.* **2020**, *381*, 122652. [[CrossRef](#)]
64. Liu, Y.; Wei, Z.; Zhong, B.; Wang, H.; Xia, L.; Zhang, T.; Duan, X.; Jia, D.; Zhou, Y.; Huang, X. O-, N-Coordinated single Mn atoms accelerating polysulfides transformation in lithium-sulfur batteries. *Energy Storage Mater.* **2021**, *35*, 12–18. [[CrossRef](#)]
65. Tian, H.; Tian, H.; Wang, S.; Chen, S.; Zhang, F.; Song, L.; Liu, H.; Liu, J.; Wang, G. High-power lithium-selenium batteries enabled by atomic cobalt electrocatalyst in hollow carbon cathode. *Nat Commun* **2020**, *11*, 5025. [[CrossRef](#)]
66. Li, C.; Wang, Y.; Li, H.; Liu, J.; Song, J.; Fusaro, L.; Hu, Z.-Y.; Chen, Y.; Li, Y.; Su, B.-L. Weaving 3D highly conductive hierarchically interconnected nanoporous web by threading MOF crystals onto multi walled carbon nanotubes for high performance Li-Se battery. *J. Energy Chem.* **2021**, *59*, 396–404. [[CrossRef](#)]
67. Liu, Y.; Si, L.; Zhou, X.; Liu, X.; Xu, Y.; Bao, J.; Dai, Z. A selenium-confined microporous carbon cathode for ultrastable lithium-selenium batteries. *J. Mater. Chem. A* **2014**, *2*, 17735–17739. [[CrossRef](#)]
68. Lai, Y.; Yongqing, G.; Zhang, Z.; Chen, W.; Li, J. Metal-organic frameworks-derived mesoporous carbon for high performance lithium-selenium battery. *Electrochim. Acta* **2014**, *146*, 134–141. [[CrossRef](#)]
69. Jin, W.-W.; Li, H.-J.; Zou, J.-Z.; Inguva, S.; Zhang, Q.; Zeng, S.-Z.; Xu, G.-Z.; Zeng, X.-R. Metal organic framework-derived carbon nanosheets with fish-scale surface morphology as cathode materials for lithium-selenium batteries. *J. Alloys Compd.* **2020**, *820*, 153084. [[CrossRef](#)]
70. Park, S.-K.; Park, J.-S.; Kang, Y.C. Selenium-infiltrated metal-organic framework-derived porous carbon nanofibers comprising interconnected bimodal pores for Li-Se batteries with high capacity and rate performance. *J. Mater. Chem. A* **2018**, *6*, 1028–1036. [[CrossRef](#)]
71. Park, S.K.; Park, J.S.; Kang, Y.C. Metal-Organic-Framework-Derived N-Doped Hierarchically Porous Carbon Polyhedrons Anchored on Crumpled Graphene Balls as Efficient Selenium Hosts for High-Performance Lithium-Selenium Batteries. *ACS Appl. Mater. Interfaces* **2018**, *10*, 16531–16540. [[CrossRef](#)]
72. Liu, T.; Jia, M.; Zhang, Y.; Han, J.; Li, Y.; Bao, S.; Liu, D.; Jiang, J.; Xu, M. Confined selenium within metal-organic frameworks derived porous carbon microcubes as cathode for rechargeable lithium-selenium batteries. *J. Power Sources* **2017**, *341*, 53–59. [[CrossRef](#)]
73. He, J.; Lv, W.; Chen, Y.; Xiong, J.; Wen, K.; Xu, C.; Zhang, W.; Li, Y.; Qin, W.; He, W. Three-dimensional hierarchical C-Co-N/Se derived from metal-organic framework as superior cathode for Li-Se batteries. *J. Power Sources* **2017**, *363*, 103–109. [[CrossRef](#)]
74. Liu, C.; Huang, X.; Wang, J.; Song, H.; Yang, Y.; Liu, Y.; Li, J.; Wang, L.; Yu, C. Hollow Mesoporous Carbon Nanocubes: Rigid-Interface-Induced Outward Contraction of Metal-Organic Frameworks. *Adv. Funct. Mater.* **2017**, *28*, 1705253. [[CrossRef](#)]
75. He, J.; Lv, W.; Chen, Y.; Xiong, J.; Wen, K.; Xu, C.; Zhang, W.; Li, Y.; Qin, W.; He, W. Direct impregnation of SeS₂ into a MOF-derived 3D nanoporous Co-N-C architecture towards superior rechargeable lithium batteries. *J. Mater. Chem. A* **2018**, *6*, 10466–10473. [[CrossRef](#)]
76. Cong, J.; Zheng, Z.; Hao, J.; You, H.; Liu, X.; Yang, H. Hierarchical cathode from hollow CoP embedded in graphene nanosheets to synergistically confine SeS₂ for advanced Li/SeS₂ batteries. *J. Alloys Compd.* **2021**, *867*, 159089. [[CrossRef](#)]
77. Deng, D. Li-ion batteries: Basics, progress, and challenges. *Energy Sci. Eng.* **2015**, *3*, 385–418. [[CrossRef](#)]
78. Liu, Q.; Su, X.; Lei, D.; Qin, Y.; Wen, J.; Guo, F.; Wu, Y.A.; Rong, Y.; Kou, R.; Xiao, X.; et al. Approaching the capacity limit of lithium cobalt oxide in lithium ion batteries via lanthanum and aluminium doping. *Nat. Energy* **2018**, *3*, 936–943. [[CrossRef](#)]
79. Lung-Hao Hu, B.; Wu, F.-Y.; Lin, C.-T.; Khlobystov, A.N.; Li, L.-J. Graphene-modified LiFePO₄ cathode for lithium ion battery beyond theoretical capacity. *Nat. Commun.* **2013**, *4*, 1687. [[CrossRef](#)] [[PubMed](#)]
80. Li, X.; Cheng, F.; Zhang, S.; Chen, J. Shape-controlled synthesis and lithium-storage study of metal-organic frameworks Zn₄O(1,3,5-benzenetribenzoate)₂. *J. Power Sources* **2006**, *160*, 542–547. [[CrossRef](#)]
81. Férey, G.; Millange, F.; Morcrette, M.; Serre, C.; Doublet, M.L.; Grenèche, J.M.; Tarascon, J.M. Mixed-valence li/fe-based metal-organic frameworks with both reversible redox and sorption properties. *Angew. Chem.* **2007**, *46*, 3259–3263. [[CrossRef](#)]
82. de Combarieu, G.; Morcrette, M.; Millange, F.; Guillou, N.; Cabana, J.; Grey, C.P.; Margiolaki, I.; Férey, G.; Tarascon, J.M. Influence of the Benzoquinone Sorption on the Structure and Electrochemical Performance of the MIL-53(Fe) Hybrid Porous Material in a Lithium-Ion Battery. *Chem. Mater.* **2009**, *21*, 1602–1611. [[CrossRef](#)]
83. Fateeva, A.; Horcajada, P.; Devic, T.; Serre, C.; Marrot, J.; Grenèche, J.-M.; Morcrette, M.; Tarascon, J.-M.; Maurin, G.; Férey, G. Synthesis, Structure, Characterization, and Redox Properties of the Porous MIL-68(Fe) Solid. *Eur. J. Inorg. Chem.* **2010**, *2010*, 3789–3794. [[CrossRef](#)]
84. Shin, J.; Kim, M.; Cirera, J.; Chen, S.; Halder, G.J.; Yersak, T.A.; Paesani, F.; Cohen, S.M.; Meng, Y.S. MIL-101(Fe) as a lithium-ion battery electrode material: A relaxation and intercalation mechanism during lithium insertion. *J. Mater. Chem. A* **2015**, *3*, 4738–4744. [[CrossRef](#)]
85. Yamada, T.; Shiraishi, K.; Kitagawa, H.; Kimizuka, N. Applicability of MIL-101(Fe) as a cathode of lithium ion batteries. *Chem. Commun.* **2017**, *53*, 8215–8218. [[CrossRef](#)]
86. Li, C.; Zhang, C.; Xie, J.; Wang, K.; Li, J.; Zhang, Q. Ferrocene-based metal-organic framework as a promising cathode in lithium-ion battery. *Chem. Eng. J.* **2021**, *404*, 126463. [[CrossRef](#)]

87. Peng, Z.; Yi, X.; Liu, Z.; Shang, J.; Wang, D. Triphenylamine-Based Metal-Organic Frameworks as Cathode Materials in Lithium-Ion Batteries with Coexistence of Redox Active Sites, High Working Voltage, and High Rate Stability. *ACS Appl. Mater. Interfaces* **2016**, *8*, 14578–14585. [[CrossRef](#)] [[PubMed](#)]
88. Nagatomi, H.; Yanai, N.; Yamada, T.; Shiraiishi, K.; Kimizuka, N. Synthesis and Electric Properties of a Two-Dimensional Metal-Organic Framework Based on Phthalocyanine. *Chemistry* **2018**, *24*, 1806–1810. [[CrossRef](#)] [[PubMed](#)]
89. Sun, P.-P.; Zhang, Y.-H.; Shi, H.; Shi, F.-N. Study on the properties of Cu powder modified 3-D Co-MOF in electrode materials of lithium ion batteries. *J. Solid State Chem.* **2022**, *307*, 122740. [[CrossRef](#)]
90. Zheng, W.; Hu, T.; Fang, Y.; Li, L.; Yuan, W. High capacity of microspheric manganese and cobalt trimesic dual-metal organic framework for Li-ion battery. *J. Solid State Chem.* **2022**, *306*, 122719. [[CrossRef](#)]
91. He, B.; Zhang, Q.; Man, P.; Zhou, Z.; Li, C.; Li, Q.; Xie, L.; Wang, X.; Pang, H.; Yao, Y. Self-sacrificed synthesis of conductive vanadium-based Metal-Organic framework nanowire-bundle arrays as binder-free cathodes for high-rate and high-energy-density wearable Zn-Ion batteries. *Nano Energy* **2019**, *64*, 103935. [[CrossRef](#)]
92. Xu, J.; Lin, F.; Doeff, M.M.; Tong, W. A review of Ni-based layered oxides for rechargeable Li-ion batteries. *J. Mater. Chem. A* **2017**, *5*, 874–901. [[CrossRef](#)]
93. Li, B.; Li, G.; Zhang, D.; Fan, J.; Chen, D.; Liu, X.; Feng, T.; Li, L. Zeolitic imidazolate framework-8 modified LiNi₁/3Co₁/3Mn₁/3O₂: A durable cathode showing excellent electrochemical performances in Li-ion batteries. *Electrochim. Acta* **2020**, *336*, 135724. [[CrossRef](#)]
94. Liang, S.; Hu, J.; Zhang, Y.; Wang, Y.; Cao, X.; Pan, A. Facile synthesis of sandwich-structured Li₃V₂(PO₄)₃/carbon composite as cathodes for high performance lithium-ion batteries. *J. Alloys Compd.* **2016**, *683*, 178–185. [[CrossRef](#)]
95. Liao, Y.; Li, C.; Lou, X.; Hu, X.; Ning, Y.; Yuan, F.; Chen, B.; Shen, M.; Hu, B. Carbon-coated Li₃V₂(PO₄)₃ derived from metal-organic framework as cathode for lithium-ion batteries with high stability. *Electrochim. Acta* **2018**, *271*, 608–616. [[CrossRef](#)]
96. Wang, Z.; He, W.; Zhang, X.; Yue, Y.; Liu, J.; Zhang, C.; Fang, L. Multilevel structures of Li₃V₂(PO₄)₃/phosphorus-doped carbon nanocomposites derived from hybrid V-MOFs for long-life and cheap lithium ion battery cathodes. *J. Power Sources* **2017**, *366*, 9–17. [[CrossRef](#)]
97. Kim, T.; Kim, H.; You, T.-S.; Kim, J. Carbon-coated V₂O₅ nanoparticles derived from metal-organic frameworks as a cathode material for rechargeable lithium-ion batteries. *J. Alloys Compd.* **2017**, *727*, 522–530. [[CrossRef](#)]
98. Zhang, Y.; Pan, A.; Wang, Y.; Wei, W.; Su, Y.; Hu, J.; Cao, G.; Liang, S. Dodecahedron-Shaped Porous Vanadium Oxide and Carbon Composite for High-Rate Lithium Ion Batteries. *ACS Appl. Mater. Interfaces* **2016**, *8*, 17303–17311. [[CrossRef](#)]
99. Xie, Y.; Chen, S.; Lin, Z.; Yang, W.; Zou, H.; Sun, R.W.-Y. Enhanced electrochemical performance of Li-rich layered oxide, Li_{1.2}Mn_{0.54}Co_{0.13}Ni_{0.13}O₂, by surface modification derived from a MOF-assisted treatment. *Electrochem. Commun.* **2019**, *99*, 65–70. [[CrossRef](#)]
100. Xiao, Z.; Meng, J.; Li, Q.; Wang, X.; Huang, M.; Liu, Z.; Han, C.; Mai, L. Novel MOF shell-derived surface modification of Li-rich layered oxide cathode for enhanced lithium storage. *Sci. Bull.* **2018**, *63*, 46–53. [[CrossRef](#)]
101. Zhao, L.; Yu, J.; Xing, C.; Ullah, Z.; Yu, C.; Zhu, S.; Chen, M.; Li, W.; Li, Q.; Liu, L. Nanopore confined anthraquinone in MOF-derived N-doped microporous carbon as stable organic cathode for lithium-ion battery. *Energy Storage Mater.* **2019**, *22*, 433–440. [[CrossRef](#)]
102. Zhao, L.; Guan, Z.; Ullah, Z.; Yu, C.; Song, H.; Chu, R.; Zhang, Y.; Li, W.; Li, Q.; Liu, L. Significantly stable organic cathode for lithium-ion battery based on nanoconfined poly(anthraquinonyl sulfide)@MOF-derived microporous carbon. *Electrochim. Acta* **2020**, *335*, 135681. [[CrossRef](#)]
103. Wang, X.; Zhang, B.; Feng, J.; Wang, L.; Wu, B.; Zhang, J.; Ou, X.; Hou, F.; Liang, J. Cu-MOF-derived and porous Cu_{0.26}V₂O₅@C composite cathode for aqueous zinc-ion batteries. *Sustain. Mater. Technol.* **2020**, *26*, e00236. [[CrossRef](#)]
104. Huo, Y.; Teng, Y.; Cai, K.; Chen, H. Honeycomb ZnO/N/C obtained from cornsilk and ZIF-8 dual induced method for long-life aqueous zinc-ion batteries. *J. Alloys Compd.* **2021**, *855*, 157398. [[CrossRef](#)]
105. Fu, Y.; Wei, Q.; Zhang, G.; Wang, X.; Zhang, J.; Hu, Y.; Wang, D.; Zuin, L.; Zhou, T.; Wu, Y.; et al. High-Performance Reversible Aqueous Zn-Ion Battery Based on Porous MnOx Nanorods Coated by MOF-Derived N-Doped Carbon. *Adv. Energy Mater.* **2018**, *8*, 1801445. [[CrossRef](#)]
106. Jia, D.; Yang, Z.; Gu, W.; Liu, X. Manganese-based metal-organic-framework derived hydrophilic cathode with carbon nanotubes introduced for long-life and high-performance aqueous zinc-ion battery. *J. Alloys Compd.* **2022**, *910*, 164876. [[CrossRef](#)]
107. Chu, R.; Song, H.; Ullah, Z.; Guan, Z.; Zhang, Y.; Zhao, L.; Chen, M.; Li, W.; Li, Q.; Liu, L. ZIF-8 derived nitrogen-doped carbon composites boost the rate performance of organic cathodes for sodium ion batteries. *Electrochim. Acta* **2020**, *362*, 137115. [[CrossRef](#)]
108. Lu, Z.; Wang, N.; Zhang, Y.; Xue, P.; Guo, M.; Tang, B.; Xu, X.; Wang, W.; Bai, Z.; Dou, S. Metal-Organic Framework-Derived Sea-Cucumber-like FeS₂@C Nanorods with Outstanding Pseudocapacitive Na-Ion Storage Properties. *ACS Appl. Energy Mater.* **2018**, *1*, 6234–6241. [[CrossRef](#)]
109. Lee, J.-S.; Tai Kim, S.; Cao, R.; Choi, N.-S.; Liu, M.; Lee, K.T.; Cho, J. Metal-Air Batteries with High Energy Density: Li-Air versus Zn-Air. *Adv. Energy Mater.* **2011**, *1*, 34–50. [[CrossRef](#)]
110. Yan, X.; Ha, Y.; Wu, R. Binder-Free Air Electrodes for Rechargeable Zinc-Air Batteries: Recent Progress and Future Perspectives. *Small Methods* **2021**, *5*, 2000827. [[CrossRef](#)] [[PubMed](#)]

111. Wang, R.; Chen, Z.; Hu, N.; Xu, C.; Shen, Z.; Liu, J. Nanocarbon-Based Electrocatalysts for Rechargeable Aqueous Li/Zn-Air Batteries. *ChemElectroChem* **2018**, *5*, 1745–1763. [[CrossRef](#)]
112. Dai, Y.; Yu, J.; Cheng, C.; Tan, P.; Ni, M. Mini-review of perovskite oxides as oxygen electrocatalysts for rechargeable zinc-air batteries. *Chem. Eng. J.* **2020**, *397*, 125516. [[CrossRef](#)]
113. Xu, L.; Wu, S.; Deng, D.; Wang, C.; Qian, J.; Lu, G.; Li, H. Fabricating highly active and stable tungsten carbide electrocatalyst for rechargeable zinc-air batteries: An approach of dual metal Co-adjusted the electronic structure. *J. Alloys Compd.* **2021**, *868*, 159236. [[CrossRef](#)]
114. Li, J.; Wan, T.; Li, J.; Zhang, Z.; Wang, Y.; Liu, G. Three-dimensionally ordered mesoporous trimetal sulfide as efficient electrocatalyst for rechargeable zinc-air batteries. *Appl. Surf. Sci.* **2022**, *575*, 151728. [[CrossRef](#)]
115. Vayenas, M.; Vaitis, C.; Sourkouni, G.; Pandis, P.K.; Argiris, C. Investigation of alternative materials as bifunctional catalysts for electrochemical applications. *Chim. Techno Acta* **2019**, *6*, 120–129. [[CrossRef](#)]
116. Wu, D.; Guo, Z.; Yin, X.; Pang, Q.; Tu, B.; Zhang, L.; Wang, Y.G.; Li, Q. Metal-organic frameworks as cathode materials for Li-O₂ batteries. *Adv. Mater.* **2014**, *26*, 3258–3262. [[CrossRef](#)]
117. Yan, W.; Guo, Z.; Xu, H.; Lou, Y.; Chen, J.; Li, Q. Downsizing metal-organic frameworks with distinct morphologies as cathode materials for high-capacity Li-O₂ batteries. *Mater. Chem. Front.* **2017**, *1*, 1324–1330. [[CrossRef](#)]
118. Kim, S.H.; Lee, Y.J.; Kim, D.H.; Lee, Y.J. Bimetallic Metal-Organic Frameworks as Efficient Cathode Catalysts for Li-O₂ Batteries. *ACS Appl. Mater. Interfaces* **2018**, *10*, 660–667. [[CrossRef](#)]
119. Shin, S.; Yoon, Y.; Shin, M.W. Co/Zn-based bimetallic MOF-derived hierarchical porous Co/C composite as cathode material for high-performance lithium-air batteries. *Int. J. Energy Res.* **2022**, *46*, 9900–9910. [[CrossRef](#)]
120. Zhang, X.; Dong, P.; Lee, J.-I.; Gray, J.T.; Cha, Y.-H.; Ha, S.; Song, M.-K. Enhanced cycling performance of rechargeable Li-O₂ batteries via LiOH formation and decomposition using high-performance MOF-74@CNTs hybrid catalysts. *Energy Storage Mater.* **2019**, *17*, 167–177. [[CrossRef](#)]
121. Shin, S.; Yoon, H.; Yoon, Y.; Park, S.; Shin, M.W. Porosity tailoring of the Zn-MOF-5 derived carbon materials and its effects on the performance as a cathode for lithium-air batteries. *Microporous Mesoporous Mater.* **2021**, *311*, 110726. [[CrossRef](#)]
122. Ge, Q.; Chen, M.; Lou, X.; Zhang, W.; Shen, M.; Yang, Q.; Hu, B. Centrifugal Field Guided Dual Templating Synthesis of Functional Macro-Microporous Carbon. *Part. Part. Syst. Charact.* **2018**, *35*, 1800262. [[CrossRef](#)]
123. Chatterjee, A.; Or, S.W. Metal-organic framework-derived MnO/CoMn₂O₄@N-C nanorods with nanoparticle interstitial decoration in core@shell structure as improved bifunctional electrocatalytic cathodes for Li-O₂ batteries. *Electrochim. Acta* **2020**, *338*, 135809. [[CrossRef](#)]
124. Zhang, P.; Li, J.; Feng, J.; Wang, Y.; Xu, A.; Chen, T.; Zhao, L.; Dang, F.; Zhang, X.; Wang, H. MOF-template derived hollow CeO₂/Co₃O₄ polyhedrons with efficient cathode catalytic capability in Li-O₂ batteries. *Chin. Chem. Lett.* **2021**, in press. [[CrossRef](#)]
125. Tan, G.; Chong, L.; Amine, R.; Lu, J.; Liu, C.; Yuan, Y.; Wen, J.; He, K.; Bi, X.; Guo, Y.; et al. Toward Highly Efficient Electrocatalyst for Li-O₂ Batteries Using Biphasic N-Doping Cobalt@Graphene Multiple-Capsule Heterostructures. *Nano Lett.* **2017**, *17*, 2959–2966. [[CrossRef](#)] [[PubMed](#)]
126. Tang, J.; Wu, S.; Wang, T.; Gong, H.; Zhang, H.; Alshehri, S.M.; Ahamad, T.; Zhou, H.; Yamauchi, Y. Cage-Type Highly Graphitic Porous Carbon-Co₃O₄ Polyhedron as the Cathode of Lithium-Oxygen Batteries. *ACS Appl. Mater. Interfaces* **2016**, *8*, 2796–2804. [[CrossRef](#)]
127. Zhao, Y.; Ding, L.; Wang, X.; Yang, X.; He, J.; Yang, B.; Wang, B.; Zhang, D.; Li, Z. Yolk-shell ZIF-8@ZIF-67 derived Co₃O₄@NiCo₂O₄ catalysts with effective electrochemical properties for Li-O₂ batteries. *J. Alloys Compd.* **2021**, *861*, 157945. [[CrossRef](#)]
128. Chen, W.; Zhang, Z.; Bao, W.; Lai, Y.; Li, J.; Gan, Y.; Wang, J. Hierarchical mesoporous γ -Fe₂O₃/carbon nanocomposites derived from metal organic frameworks as a cathode electrocatalyst for rechargeable Li-O₂ batteries. *Electrochim. Acta* **2014**, *134*, 293–301. [[CrossRef](#)]
129. Gan, Y.; Lai, Y.; Zhang, Z.; Chen, W.; Du, K.; Li, J. Hierarchical Cr₂O₃@OPC composites with octahedral shape for rechargeable nonaqueous lithium-oxygen batteries. *J. Alloys Compd.* **2016**, *665*, 365–372. [[CrossRef](#)]
130. Chen, K.; Yang, D.-Y.; Huang, G.; Zhang, X.-B. Lithium-Air Batteries: Air-Electrochemistry and Anode Stabilization. *Acc. Chem. Res.* **2021**, *54*, 632–641. [[CrossRef](#)] [[PubMed](#)]
131. Sun, H.; Chen, G.; Zhu, Y.; Liu, B.; Zhou, W.; Shao, Z. B-Site Cation Ordered Double Perovskites as Efficient and Stable Electrocatalysts for Oxygen Evolution Reaction. *Chemistry* **2017**, *23*, 5722–5728. [[CrossRef](#)] [[PubMed](#)]
132. Hua, B.; Sun, Y.-F.; Li, M.; Yan, N.; Chen, J.; Zhang, Y.-Q.; Zeng, Y.; Shalchi Amirkhiz, B.; Luo, J.-L. Stabilizing Double Perovskite for Effective Bifunctional Oxygen Electrocatalysis in Alkaline Conditions. *Chem. Mater.* **2017**, *29*, 6228–6237. [[CrossRef](#)]
133. Mai, Z.; Duan, W.; Wang, K.; Tang, Z.; Chen, S. Integrating ZnCo₂O₄ submicro/nanospheres with CoxSe_y nanosheets for the oxygen evolution reaction and zinc-air batteries. *Sustain. Energy Fuels* **2020**, *4*, 2184–2191. [[CrossRef](#)]
134. Gao, Z.W.; Liu, J.Y.; Chen, X.M.; Zheng, X.L.; Mao, J.; Liu, H.; Ma, T.; Li, L.; Wang, W.C.; Du, X.W. Engineering NiO/NiFe LDH Intersection to Bypass Scaling Relationship for Oxygen Evolution Reaction via Dynamic Tridimensional Adsorption of Intermediates. *Adv. Mater.* **2019**, *31*, e1804769. [[CrossRef](#)] [[PubMed](#)]

135. Huang, K.; Guo, S.; Wang, R.; Lin, S.; Hussain, N.; Wei, H.; Deng, B.; Long, Y.; Lei, M.; Tang, H.; et al. Two-dimensional MOF/MOF derivative arrays on nickel foam as efficient bifunctional coupled oxygen electrodes. *Chin. J. Catal.* **2020**, *41*, 1754–1760. [[CrossRef](#)]
136. Wang, Y.; Tao, L.; Xiao, Z.; Chen, R.; Jiang, Z.; Wang, S. 3D Carbon Electrocatalysts In Situ Constructed by Defect-Rich Nanosheets and Polyhedrons from NaCl-Sealed Zeolitic Imidazolate Frameworks. *Adv. Funct. Mater.* **2018**, *28*, 1705356. [[CrossRef](#)]
137. Yang, M.; Hu, X.; Fang, Z.; Sun, L.; Yuan, Z.; Wang, S.; Hong, W.; Chen, X.; Yu, D. Bifunctional MOF-Derived Carbon Photonic Crystal Architectures for Advanced Zn–Air and Li–S Batteries: Highly Exposed Graphitic Nitrogen Matters. *Adv. Funct. Mater.* **2017**, *27*, 1701971. [[CrossRef](#)]
138. Yan, J.; Zheng, X.; Wei, C.; Sun, Z.; Zeng, K.; Shen, L.; Sun, J.; Rummeli, M.H.; Yang, R. Nitrogen-doped hollow carbon polyhedron derived from salt-encapsulated ZIF-8 for efficient oxygen reduction reaction. *Carbon* **2021**, *171*, 320–328. [[CrossRef](#)]
139. Xu, K.; Bao, H.; Tang, C.; Maliutina, K.; Li, F.; Fan, L. Engineering hierarchical MOFs-derived Fe–N–C nanostructure with improved oxygen reduction activity for zinc-air battery: The role of iron oxide. *Mater. Today Energy* **2020**, *18*, 100500. [[CrossRef](#)]
140. Zhang, Z.; Jin, H.; Zhu, J.; Li, W.; Zhang, C.; Zhao, J.; Luo, F.; Sun, Z.; Mu, S. 3D flower-like ZnFe-ZIF derived hierarchical Fe, N-Codoped carbon architecture for enhanced oxygen reduction in both alkaline and acidic media, and zinc-air battery performance. *Carbon* **2020**, *161*, 502–509. [[CrossRef](#)]
141. Jin, H.; Zhou, H.; Li, W.; Wang, Z.; Yang, J.; Xiong, Y.; He, D.; Chen, L.; Mu, S. In situ derived Fe/N/S-codoped carbon nanotubes from ZIF-8 crystals as efficient electrocatalysts for the oxygen reduction reaction and zinc–air batteries. *J. Mater. Chem. A* **2018**, *6*, 20093–20099. [[CrossRef](#)]
142. Liu, Z.; Liu, J.; Wu, H.B.; Shen, G.; Le, Z.; Chen, G.; Lu, Y. Iron-decorated nitrogen-rich carbons as efficient oxygen reduction electrocatalysts for Zn-air batteries. *Nanoscale* **2018**, *10*, 16996–17001. [[CrossRef](#)] [[PubMed](#)]
143. Zhang, X.; Han, X.; Jiang, Z.; Xu, J.; Chen, L.; Xue, Y.; Nie, A.; Xie, Z.; Kuang, Q.; Zheng, L. Atomically dispersed hierarchically ordered porous Fe–N–C electrocatalyst for high performance electrocatalytic oxygen reduction in Zn-Air battery. *Nano Energy* **2020**, *71*, 104547. [[CrossRef](#)]
144. Chen, K.; Ci, S.; Xu, Q.; Cai, P.; Li, M.; Xiang, L.; Hu, X.; Wen, Z. Iron-incorporated nitrogen-doped carbon materials as oxygen reduction electrocatalysts for zinc-air batteries. *Chin. J. Catal.* **2020**, *41*, 858–867. [[CrossRef](#)]
145. Han, H.; Chao, S.; Bai, Z.; Wang, X.; Yang, X.; Qiao, J.; Chen, Z.; Yang, L. Metal-Organic-Framework-Derived Co Nanoparticles Deposited on N-Doped Bimodal Mesoporous Carbon Nanorods as Efficient Bifunctional Catalysts for Rechargeable Zinc–Air Batteries. *ChemElectroChem* **2018**, *5*, 1868–1873. [[CrossRef](#)]
146. Li, J.-C.; Wu, X.-T.; Chen, L.-J.; Li, N.; Liu, Z.-Q. Bifunctional MOF-derived Co-N-doped carbon electrocatalysts for high-performance zinc-air batteries and MFCs. *Energy* **2018**, *156*, 95–102. [[CrossRef](#)]
147. Amiin, I.S.; Liu, X.; Pu, Z.; Li, W.; Li, Q.; Zhang, J.; Tang, H.; Zhang, H.; Mu, S. From 3D ZIF Nanocrystals to Co-Nx/C Nanorod Array Electrocatalysts for ORR, OER, and Zn-Air Batteries. *Adv. Funct. Mater.* **2018**, *28*, 1704638. [[CrossRef](#)]
148. Zhang, M.; Dai, Q.; Zheng, H.; Chen, M.; Dai, L. Novel MOF-Derived Co@N-C Bifunctional Catalysts for Highly Efficient Zn-Air Batteries and Water Splitting. *Adv. Mater.* **2018**, *30*, 1705431. [[CrossRef](#)] [[PubMed](#)]
149. Zang, W.; Sumboja, A.; Ma, Y.; Zhang, H.; Wu, Y.; Wu, S.; Wu, H.; Liu, Z.; Guan, C.; Wang, J.; et al. Single Co Atoms Anchored in Porous N-Doped Carbon for Efficient Zinc–Air Battery Cathodes. *ACS Catal.* **2018**, *8*, 8961–8969. [[CrossRef](#)]
150. Chen, S.; Shu, X.; Wang, H.; Zhang, J. Thermally driven phase transition of manganese oxide on carbon cloth for enhancing the performance of flexible all-solid-state zinc–air batteries. *J. Mater. Chem. A* **2019**, *7*, 19719–19727. [[CrossRef](#)]
151. Chen, D.; Yu, J.; Cui, Z.; Zhang, Q.; Chen, X.; Sui, J.; Dong, H.; Yu, L.; Dong, L. Hierarchical architecture derived from two-dimensional zeolitic imidazolate frameworks as an efficient metal-based bifunctional oxygen electrocatalyst for rechargeable Zn–air batteries. *Electrochim. Acta* **2020**, *331*, 135394. [[CrossRef](#)]
152. Zhou, L.; Zhou, P.; Zhang, Y.; Liu, B.; Gao, P.; Guo, S. 3D star-like atypical hybrid MOF derived single-atom catalyst boosts oxygen reduction catalysis. *J. Energy Chem.* **2021**, *55*, 355–360. [[CrossRef](#)]
153. Zhou, D.; Fu, H.; Long, J.; Shen, K.; Gou, X. Novel fusiform core-shell-MOF derived intact metal@carbon composite: An efficient cathode catalyst for aqueous and solid-state Zn-air batteries. *J. Energy Chem.* **2022**, *64*, 385–394. [[CrossRef](#)]
154. Huo, M.; Wang, B.; Zhang, C.; Ding, S.; Yuan, H.; Liang, Z.; Qi, J.; Chen, M.; Xu, Y.; Zhang, W.; et al. 2D Metal-Organic Framework Derived CuCo Alloy Nanoparticles Encapsulated by Nitrogen-Doped Carbonaceous Nanoleaves for Efficient Bifunctional Oxygen Electrocatalyst and Zinc-Air Batteries. *Chemistry* **2019**, *25*, 12780–12788. [[CrossRef](#)]
155. Zhao, Y.; Zhang, H.-M.; Zhang, Y.; Zhang, M.; Yu, J.; Liu, H.; Yu, Z.; Yang, B.; Zhu, C.; Xu, J. Leaf-like 2D nanosheet as efficient oxygen reduction reaction catalyst for Zn-air battery. *J. Power Sources* **2019**, *434*, 226717. [[CrossRef](#)]
156. Zhong, Y.; Pan, Z.; Wang, X.; Yang, J.; Qiu, Y.; Xu, S.; Lu, Y.; Huang, Q.; Li, W. Hierarchical Co₃O₄ Nano-Micro Arrays Featuring Superior Activity as Cathode in a Flexible and Rechargeable Zinc-Air Battery. *Adv. Sci.* **2019**, *6*, 1802243. [[CrossRef](#)]
157. Wei, W.; Shi, X.; Gao, P.; Wang, S.; Hu, W.; Zhao, X.; Ni, Y.; Xu, X.; Xu, Y.; Yan, W.; et al. Well-elaborated, mechanochemically synthesized Fe-TPP@ZIF precursors (Fe-TPP = tetraphenylporphine iron) to atomically dispersed iron–nitrogen species for oxygen reduction reaction and Zn-air batteries. *Nano Energy* **2018**, *52*, 29–37. [[CrossRef](#)]
158. Jiang, M.; Yang, J.; Ju, J.; Zhang, W.; He, L.; Zhang, J.; Fu, C.; Sun, B. Space-confined synthesis of CoNi nanoalloy in N-doped porous carbon frameworks as efficient oxygen reduction catalyst for neutral and alkaline aluminum-air batteries. *Energy Storage Mater.* **2020**, *27*, 96–108. [[CrossRef](#)]

159. Li, D.; Sun, L.; Hu, L.; Zhu, J.; Shi, J.; Guo, D. Rare earth insitu-doped ZIF-67 derived N doped C encapsulated Sm₂O₃/Co nanoparticles as excellent oxygen reduction reaction catalyst for Al-air batteries. *J. Power Sources* **2021**, *482*, 229052. [[CrossRef](#)]
160. Liu, Y.; Jiang, H.; Hao, J.; Liu, Y.; Shen, H.; Li, W.; Li, J. Metal-Organic Framework-Derived Reduced Graphene Oxide-Supported ZnO/ZnCo₂O₄/C Hollow Nanocages as Cathode Catalysts for Aluminum-O₂ Batteries. *ACS Appl. Mater. Interfaces* **2017**, *9*, 31841–31852. [[CrossRef](#)]
161. Li, J.; Zhou, N.; Song, J.; Fu, L.; Yan, J.; Tang, Y.; Wang, H. Cu-MOF-Derived Cu/Cu₂O Nanoparticles and Cu_NxCy Species to Boost Oxygen Reduction Activity of Ketjenblack Carbon in Al-Air Battery. *ACS Sustain. Chem. Eng.* **2017**, *6*, 413–421. [[CrossRef](#)]